HAL
open science

The forced precession of the Moon's inner core

Mathieu Dumberry, Mark Wieczorek

To cite this version:

Mathieu Dumberry, Mark Wieczorek. The forced precession of the Moon's inner core. Journal of Geophysical Research. Planets, 2016, 121 (7), pp.1264-1292. 10.1002/2015JE004986 . hal-02458619

HAL Id: hal-02458619

https://hal.science/hal-02458619v1

Submitted on 26 Jun 2020

HAL is a multi-disciplinary open access archive for the deposit and dissemination of scientific research documents, whether they are published or not. The documents may come from teaching and research institutions in France or abroad, or from public or private research centers.

L'archive ouverte pluridisciplinaire **HAL**, est destinée au dépôt et à la diffusion de documents scientifiques de niveau recherche, publiés ou non, émanant des établissements d'enseignement et de recherche français ou étrangers, des laboratoires publics ou privés.

AGU PUBLICATIONS

JGR

Journal of Geophysical Research: Planets

RESEARCH ARTICLE

10.1002/2015JE004986

Key Points:
- The Moon's inner core is forced to precess with an 18.6 year period
- The inner core tilt angle of precession is tied to the free inner core nutation frequency
- The present-day tilt with respect to the mantle may be 2 to 5 degrees

Correspondence to:
M. Dumberry,
dumberry@ualberta.ca

Citation:
Dumberry, M., and M. A. Wieczorek (2016), The forced precession of the Moon's inner core, *J. Geophys. Res. Planets*, *121*, 1264–1292, doi:10.1002/2015JE004986.

Received 13 DEC 2015
Accepted 20 MAY 2016
Accepted article online 13 JUN 2016
Published online 14 JUL 2016

©2016. American Geophysical Union. All Rights Reserved.

The forced precession of the Moon's inner core

Mathieu Dumberry[1,2] and Mark A. Wieczorek[3]

[1]Department of Physics, University of Alberta, Edmonton, Alberta, Canada, [2]ISTerreUniversité Grenoble-Alpes, Grenoble, France, [3]Institut de Physique du Globe, Paris, France

Abstract The tilt angle of the 18.6 year precession of the Moon's solid inner core is unknown, but it is set by a balance between gravitational and pressure torques acting on its elliptical figure. We show here that to first order, the angle of precession of the inner core of a planetary body is determined by the frequency of the free inner core nutation, ω_{ficn}, relative to the precession frequency, Ω_p. If $|\omega_{\text{ficn}}| \ll |\Omega_p|$, the inner core is blind to the gravitational influence of the mantle. If $|\omega_{\text{ficn}}| \gg |\Omega_p|$, the inner core is gravitationally locked to the mantle and is nearly aligned with it. If $\omega_{\text{ficn}} \approx \Omega_p$, large inner core tilt angles can result from resonant excitation. Viscous inner core relaxation and electromagnetic coupling can attenuate large tilt angles. For the specific case of the Moon, we show that ω_{ficn} is to within a factor of 2 of $\Omega_p = 2\pi/18.6\ \text{yr}^{-1}$. For a rigid inner core, this implies a tilt of 2 to 5° with respect to the mantle, and larger if ω_{ficn} is very close to Ω_p. More modest tilt angles between 0 and 0.5° result if viscous relaxation within the inner core occurs on a timescale of one lunar day. Predictions from our model may be used in an attempt to detect the gravity signal resulting from a tilted inner core, to determine the past history of the inner core tilt angle, and to assess models of dynamo generation powered by differential rotation at the core-mantle and inner core boundaries.

1. Introduction

Several aspects of the rotational dynamics of the Moon are well established. The rotation period of its solid mantle is synchronous to its period of revolution around the Earth. The orbital plane of the Moon is inclined by an angle $I = 5.145°$ with respect to the ecliptic plane and precesses in a retrograde direction with a period of 18.6 years. Lunar laser ranging observations [*Dickey et al.*, 1994] have revealed that the spin symmetry axis of the Moon is tilted by an angle $\theta_p = 1.543°$ with respect to the ecliptic, in the opposite direction of I, and also precesses in a retrograde direction with the same 18.6 year period (Figure 1). The tilt θ_p results from the gravitational torque that Earth exerts on the elliptical figure of the Moon. This configuration describes a Cassini state, whereby the spin-symmetry axis and the normal to the orbital plane remain coplanar with, and are precessing about, the normal to the ecliptic [*Colombo*, 1966; *Peale*, 1969]. Observations suggest that the spin vector lags behind an exact Cassini state by a very small angle of 0.26 arc sec, indicating the presence of a dissipation mechanism [*Yoder*, 1981; *Williams et al.*, 2001].

The observed tilt angle of precession θ_p does not characterize the full Moon, but only the visible solid outer region made up of its mantle and crust. As summarized by *Wieczorek et al.* [2006], various lines of evidence suggest that the Moon has a small metallic core and that its outer portion is molten today. Whether the fluid core follows the precession of the mantle depends on the pressure torque exerted on the elliptical shape of the core-mantle boundary (CMB) by its misaligned rotation vector. This pressure torque is proportional to the CMB flattening (i.e., the pole-to-equator topography) which is believed to be too small in the Moon today for an entrainment of the fluid core [*Poincaré*, 1910; *Goldreich*, 1967]. An equivalent and complementary way to express this is to consider the free precession frequency of a misaligned rotation vector of the fluid core about the symmetry axis of the mantle resulting from this pressure torque. For Earth, this rotational mode is called the free core nutation (FCN), and we use this terminology here. The FCN period of the Moon is not known but estimated to be longer than ~150 years [e.g., *Gusev and Petrova*, 2008; *Williams et al.*, 2014a], much longer than the 18.6 year period of mantle precession. This implies that the fluid core does not have time to adjust to the precession motion of the mantle and is not efficiently entrained. The rotation vector of the fluid core should therefore remain in close alignment with the normal to the ecliptic, though its precise angle is not observed directly and is unknown. When the Moon was considerably closer to Earth in its past, the FCN could

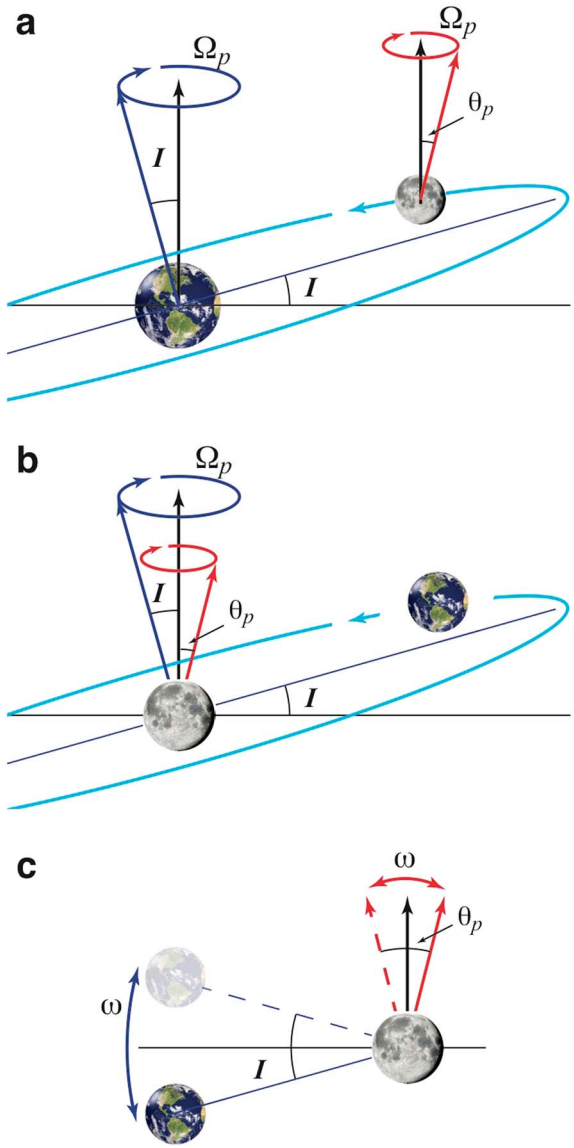

Figure 1. Earth-Moon orbital dynamics. (a) The Moon's 27.322 day orbit around the Earth (light blue) is inclined by an angle $I = 5.145°$ with respect to the ecliptic (dark blue vector) and precesses in a retrograde direction at a frequency of $\Omega_p = 2\pi/18.6\ \mathrm{yr}^{-1}$ (dark blue circular motion). The symmetry axis of the Moon's mantle (red vector) is inclined by $\theta_p = 1.543°$ with respect to the ecliptic, in the same plane as I but in the opposite direction, and is also precessing (red circular motion) at frequency Ω_p. (b) Viewed from a frame centered on the Moon, the Earth traces a 27.322 day orbit around the Moon, inclined by I and precessing at frequency Ω_p. (c) In a frame centered on the Moon, rotating at $\Omega_o = 2\pi/27.322\ \mathrm{day}^{-1}$ about the ecliptic normal, and when only considering the mean torque averaged over one lunar orbit, the Earth remains at a fixed longitude point, but I and θ_p oscillate at frequency $\omega = -\Omega_o - \Omega_p = -2\pi/27.212\ \mathrm{day}^{-1}$.

have been faster than the mantle precession frequency, causing the rotation of the fluid core to be locked to the mantle [*Meyer and Wisdom*, 2011].

Thermal evolution models suggest that a portion of the core should have crystallized to form a solid inner core at its center [*Zhang et al.*, 2013; *Laneuville et al.*, 2014; *Scheinberb et al.*, 2015]. Just as the gravitational torque from Earth forces the tilt θ_p of the mantle, it should also entrain a tilt of the elliptical figure of the solid inner core, forcing it to precess also with a 18.6 year period. In other words, there is an equivalent Cassini state for the inner core. The total torque on the inner core also includes a pressure torque at the inner core boundary (ICB) if it is misaligned with the rotation vector of the fluid core and a gravitational torque from a misalignment with the mantle. The tilt angle of precession of the inner core is that which allows to balance the combination

of these torques and thus depends on their relative importance [*Williams*, 2007]. Further, the gravitational torque exerted by the inner core on the mantle may affect the Cassini state of the latter [e.g., *Peale et al.*, 2016].

Whereas the basic description of the precession dynamic of a fluid shell enclosed by an elliptical mantle has been presented by *Poincaré* [1910] more than a hundred years ago, few studies have focused on the precession of solid inner cores. Our main motivation in this study is to address this gap and expose a few fundamental aspects of the precession of inner cores of moons and planets. In particular, by analogy with the FCN frequency, which determines the threshold between a fluid core that is locked or decoupled to the mantle precession, we want to identify a similar criterion to yield a first-order picture of the precession angle of the inner core. We show here that gravitational locking (i.e., near perfect alignment) of the inner core figure to that of the mantle depends on the frequency of another free mode, the free inner core nutation (FICN).

To do so, we present a dynamical model of the precession dynamics of a planetary body that comprises both a fluid and solid core. We assume that both the mantle and inner core are axially symmetric, though they can be misaligned, and we neglect elastic deformations. These simplifications allow us to focus on the precession dynamics, without the added complication of longitudinal librations (both free and forced) associated with triaxial bodies [e.g., *Eckhardt*, 1981]. Further, our model is developed under the assumption of small tilt angles. The main advantage of adopting these simplifications is that the first-order dynamics of the precession of the inner core is captured by a relatively simple set of linear equations.

The second motivation is to apply our model to determine the present-day precession tilt of the Moon's inner core. This question is important in view of recent suggestions that the Moon's past dynamo may have been powered by the misalignment of the rotation axes of the mantle and fluid core which was greater than today [*Dwyer et al.*, 2011]. If correct, a misalignment between the rotation axes of the fluid core and inner core also has the potential to power a dynamo. If, however, the differential velocity at the ICB for the present-day Moon is found to be greater than that at the CMB in the past when it was deemed sufficient for dynamo action, this would present a potential problem for this mechanism. Conversely, the absence of a dynamo today could be used as a constraint for the maximum differential velocity at the ICB that is required for dynamo generation. The Moon being really a triaxial body, our axially symmetric model cannot capture its rich spectrum of rotational dynamics. Nevertheless, our model allows to obtain a first-order picture of the inner core tilt. We show here that for a range of possible interior models, the period of the FICN for the present-day Moon is close to the forcing period of 18.6 years. By resonant excitation, the misalignment angle between the solid inner core and mantle could in fact be quite large.

The third motivation is to lay the foundation for a possible detection of the inner core of the Moon through geodetic observations. A solid inner core with a radius of 240 ± 10 km has been suggested based on one analysis of the Apollo seismic data [*Weber et al.*, 2011], but this result is equivocal [*Garcia et al.*, 2011]. In the frame attached to the rotating mantle, a misaligned inner core would be seen as precessing with a period of 1 lunar day. This would cause a periodic variation in the degree 2 order 1 coefficients of the lunar gravity field which could in principle be detected by high-precision observations obtained from the Gravity Recovery and Interior Laboratory (GRAIL) mission [*Williams*, 2007; *Zuber et al.*, 2013]. If above the GRAIL detection level, this signal would confirm the presence of a solid inner core and help constrain the deepest interior structure of the Moon. If a solid inner core were present, it would influence the libration dynamics of the Moon by the introduction of additional free modes of librations. Such signals might be detectable through careful observations of the Moon's librations via lunar laser ranging [e.g., *Williams et al.*, 2001].

Though the application of our model is focused here on the present-day Moon, our model can also be used to predict the past nature of the Cassini state as a function of the distance between Earth and the Moon. Our model is also easily generalizable to other moons and planets in a Cassini state, such as Mercury [*Peale et al.*, 2016], or even to study the precession of the inner cores of freely precessing planetary bodies (such as Earth). Furthermore, our model can also be applied to other bodies that have a solid-liquid-solid structure, such as the icy satellites of Jupiter and Saturn [e.g., *Baland et al.*, 2012].

2. Theory

In this section we develop our model of the rotational dynamics of a three-layer planetary body. The precession dynamics of the solid inner core depends on the sum of the torques acting on it. Our objective is to extract some of its general dynamical features. Since part of our objective is also to determine the tilt angle of

the inner core of the present-day Moon, we cast the description of our model to the specific case of the Moon. That is, the forcing is determined by the specific geometry of the Earth-Moon system and, when needed, chosen parameter values are those appropriate for the Moon. Our model further requires knowledge of density and flattening profiles as a function of radius, and we describe how we constrain these on the basis of lunar observations.

2.1. Precession of the Lunar Orbit and the Torque From Earth

The orbit normal of the Moon is inclined by an angle $I = 5.145°$ with respect to the ecliptic normal and precesses in a retrograde direction with a period of 18.6 years (or frequency of $\Omega_p = 2\pi/18.6\ \mathrm{yr}^{-1}$) (Figure 1a). The gravitational torque from Earth acting on the elliptical figure of the Moon's mantle leads to a tilt of its symmetry axis with respect to the ecliptic normal. Since the orbital plane of the Moon is in precession around Earth, the direction of the mean torque from Earth varies over the precessional cycle. This entrains the tilt of the mantle axis also to undergo a retrograde 18.6 year precession. In the absence of dissipation, the orbit normal, ecliptic normal, and the tilt of the Moon's mantle axis are coplanar, an arrangement that describes a Cassini state.

Although the rotation and symmetry axes of the mantle should remain in close alignment, they do not coincide exactly. This distinction is important because the gravitational torque from Earth depends on the orientation of the symmetry axis of the mantle and not on the orientation of its rotation axis. We define the direction of the ecliptic normal as $\hat{\mathbf{e}}_3$. The vector defining the orientation of the symmetry axis of the mantle is expressed by $\hat{\mathbf{e}}_3^{\mathbf{p}} = \hat{\mathbf{e}}_3 + \mathbf{p}$. For $|\mathbf{p}| \ll \mathbf{1}$, $\mathbf{p}$ corresponds to the tilt angle of the symmetry axis of the mantle with respect to the ecliptic normal; we refer to this angle as θ_p. The observed tilt of the mantle's rotation vector of $\theta_p = 1.543°$ is that which provides the balance between the change in angular momentum for the rotating and precessing Moon and the torque from Earth.

We define the rotation vector of the mantle as

$$\mathbf{\Omega} = \Omega_o(\hat{\mathbf{e}}_3 + \mathbf{p} + \mathbf{m}) \equiv \Omega_o(\hat{\mathbf{e}}_3^{\mathbf{p}} + \mathbf{m}) \equiv \Omega_o\hat{\mathbf{e}}_3^{\mathbf{p}} + \boldsymbol{\omega}_{\mathbf{m}}\,, \tag{1}$$

where $\Omega_o = 2.6617\times10^{-6}\ \mathrm{s}^{-1}$ (corresponding to a period of 27.322 days, or one sidereal month). The quantity $\boldsymbol{\omega}_{\mathbf{m}} = \Omega_o\mathbf{m}$ captures the deviation of the mantle rotation vector from an alignment with the mantle symmetry axis. For $|\mathbf{p} + \mathbf{m}| \ll 1$, $\mathbf{p} + \mathbf{m}$ corresponds to the tilt angle of the rotation axis of the mantle with respect to the ecliptic normal; we define this angle as θ_m.

In a reference frame centered on the Moon, it is the Earth that traces an orbit inclined by angle I, precessing in a retrograde direction (Figure 1b). To express the force balance involved in the Cassini state, it is further convenient to define a Moon-centered frame which is also rotating at the mean rotation rate Ω_o about the ecliptic normal $\hat{\mathbf{e}}_3$ (Figure 1c). In this frame, because of the synchronous rotation of the Moon around Earth, Earth remains on a fixed longitudinal plane, and both the orbit normal and rotation vector of the Moon oscillate in this plane respectively from $\pm I$ and $\pm\theta_p$ with frequency $-\Omega_o - \Omega_p = -2\pi/27.212\ \mathrm{day}^{-1}$ (Figure 1c). This latter depiction is only correct if the torque on the Moon is restricted to the mean torque from Earth averaged over one lunar orbit. In reality, the half-period modulation of the Earth torque and the small longitudinal librations induced by the lunar orbit's eccentricity lead to variations in the orientation of the longitudinal plane of the Earth.

Expressed in the Moon-centered frame, oriented with the ecliptic normal and rotating at Ω_o, the evolution of the angular momentum of the whole Moon $\mathbf{H}$ must obey

$$\frac{\mathrm{d}}{\mathrm{d}t}\mathbf{H} + \Omega_o\hat{\mathbf{e}}_3 \times \mathbf{H} = \mathbf{\Gamma}\,, \tag{2}$$

where $\mathbf{\Gamma}$ is the gravitational torque from Earth acting on the Moon. This equation determines the angle of tilt θ_p of the precessing mantle with respect to the ecliptic normal. If the Moon were a single rigid body, and if one assumes $\mathbf{m} = \mathbf{0}$, then $\theta_p \equiv \theta_m$. The solution to equation (2) corresponds to the Cassini state of this rigid Moon. For a Moon composed of a mantle, fluid core, and solid inner core, the situation is more complex. The gravitational torque from Earth in equation (2) acts on the Moon's mantle and leads to its tilted orientation $\hat{\mathbf{e}}_3^{\mathbf{p}}$. It also acts on the Moon's solid inner core resulting in an analogous tilt of its symmetry axis which we define as $\hat{\mathbf{e}}_3^{\mathbf{s}}$. In general, $\hat{\mathbf{e}}_3^{\mathbf{s}}$ differs from $\hat{\mathbf{e}}_3^{\mathbf{p}}$, and this induces a gravitational torque between the inner core and mantle. The tilts of the mantle and solid inner core further lead to pressure torques on the elliptical shapes of

the CMB and ICB. These internal torques participate in the overall angular momentum dynamics of the Moon and, in turn, can influence the tilt angle of the mantle with respect to the ecliptic. Hence, equation (2) must be supplemented by a model that captures the internal coupling dynamics, which we turn to next.

2.2. Internal Coupling Dynamics

To model the coupling between the Moon's interior region, we take advantage of the framework developed in *Mathews et al.* [1991a] and updated in *Mathews et al.* [2002] to model the forced nutations of Earth. This model describes the rotational response of Earth to the external torques from the Sun, Moon, and other planets acting on its elliptical figure. We adapt this model here to describe the behavior of the Moon in response to external torques. We assume an axisymmetric, rotating Moon composed of a mantle, a fluid outer core, and a solid inner core. In section 2.6 we will add a crust as a separate region, though for the purpose of rotational dynamics, the crust and mantle move as a solid body.

The nutation model of *Mathews et al.* [1991a] describes perturbations with respect to the symmetry axis of the mantle. Our frame of reference for this part of the model is one which is rotating at Ω_o and attached to the symmetry axis of the mantle $\hat{\mathbf{e}}_3^{\mathbf{p}}$. (Note that this is different from the $\hat{\mathbf{e}}_3$ frame chosen for equation (2)). The reference equilibrium state is one of uniform rotation $\mathbf{\Omega}_o = \Omega_o \hat{\mathbf{e}}_3^{\mathbf{p}}$ of all three regions aligned with the symmetry axis of the mantle. External torques ($\mathbf{\Gamma}$) lead to changes in the orientation of the rotation vectors of the mantle, fluid core, and solid inner core with respect to $\hat{\mathbf{e}}_3^{\mathbf{p}}$. The symmetry axis of the inner core is allowed to be misaligned from its rotation axis and constitutes a fourth unknown. These are found by solving a system of four equations: the first three describing respectively the evolution of the angular momentum of the whole Moon ($\mathbf{H}$), the fluid outer core ($\mathbf{H_f}$), and solid inner core ($\mathbf{H_s}$), and a fourth for the kinematic relation governing the tilt of the solid inner core relative to the mantle,

$$\frac{\mathrm{d}}{\mathrm{d}t}\mathbf{H} + \mathbf{\Omega} \times \mathbf{H} = \mathbf{\Gamma}\,, \tag{3a}$$

$$\frac{\mathrm{d}}{\mathrm{d}t}\mathbf{H_f} - \boldsymbol{\omega}_\mathbf{f} \times \mathbf{H_f} = -\mathbf{\Gamma}_\mathbf{icb}\,, \tag{3b}$$

$$\frac{\mathrm{d}}{\mathrm{d}t}\mathbf{H_s} + \mathbf{\Omega} \times \mathbf{H_s} = \mathbf{\Gamma_s} + \mathbf{\Gamma}_\mathbf{icb}\,, \tag{3c}$$

$$\frac{\mathrm{d}}{\mathrm{d}t}\mathbf{n_s} + \hat{\mathbf{e}}_3^{\mathbf{p}} \times \left(\frac{\mathbf{n_s}}{\tau} + \boldsymbol{\omega}_\mathbf{s}\right) = \mathbf{0}\,. \tag{3d}$$

In these equations, $\mathbf{\Gamma_s}$ is the total gravitational and pressure torque exerted on a tilted inner core, and $\mathbf{\Gamma}_\mathbf{icb}$ is the torque from viscous and electromagnetic surface tractions at the ICB. Because of the very small molecular viscosity of molten iron appropriate for fluid planetary cores, the torque from viscous forces is orders of magnitude smaller than the pressure and gravitational torques and we neglect it here. Note, however, that turbulence could lead to a much larger effective viscosity, in which case the viscous torque could be important at both the ICB and CMB [e.g., *Yoder*, 1981; *Williams et al.*, 2001].

The rotation vector of the mantle is defined as $\mathbf{\Omega} = \mathbf{\Omega_o} + \boldsymbol{\omega}_\mathbf{m} = \Omega_o\left(\hat{\mathbf{e}}_3^{\mathbf{p}} + \mathbf{m}\right)$, such that $\boldsymbol{\omega}_\mathbf{m} = \Omega_o\mathbf{m}$ is the small perturbation in rotation from an alignment with $\hat{\mathbf{e}}_3^{\mathbf{p}}$. The vectors $\boldsymbol{\omega}_\mathbf{f} = \Omega_o\mathbf{m_f}$ and $\boldsymbol{\omega}_\mathbf{s} = \Omega_o\mathbf{m_s}$ describe, respectively, the perturbations in the rotation of the fluid core and solid inner core with respect to the rotation vector of the mantle $\mathbf{\Omega}$. The tilt of the symmetry axis of the inner core $\mathbf{n_s} = \hat{\mathbf{e}}_3^{\mathbf{s}} - \hat{\mathbf{e}}_3^{\mathbf{p}}$ is defined as the difference between the unit vectors $\hat{\mathbf{e}}_3^{\mathbf{s}}$ (pointing in the direction of the symmetry axis of the inner core) and $\hat{\mathbf{e}}_3^{\mathbf{p}}$. In equation (3d), the term that involves $\mathbf{n_s}/\tau$ is not present in the model of *Mathews et al.* [1991a]; it has been added here to take into account viscous relaxation of the inner core with a characteristic *e*-folding time of τ. Note that this is a simplified way to prescribe this effect; see, for example, *Koot and Dumberry* [2011] for a more general framework.

2.3. A Model of the Forced Precession of the Moon

Equations (2) and (3) capture the response of the Moon subject to the torque from Earth at a given frequency. Equation (2) determines the tilt of the mantle symmetry axis with respect to ecliptic ($\mathbf{p}$); the system of equations (3) determines the inner core tilt ($\mathbf{n_s}$) and the perturbations in the spin vectors of the mantle ($\mathbf{m}$), fluid core ($\mathbf{m_f}$), and inner core ($\mathbf{m_s}$) with respect to the mantle symmetry axis. To be precise, both $\mathbf{n_s}$ and $\mathbf{m}$ are defined with respect to the symmetry axis of the mantle, while $\mathbf{m_f}$ and $\mathbf{m_s}$ are defined with respect to the perturbed rotation axis of the mantle ($\hat{\mathbf{e}}_3^{\mathbf{p}} + \mathbf{m}$). The five rotation variables $\mathbf{p}$, $\mathbf{m}$, $\mathbf{m_f}$, $\mathbf{m_s}$, and $\mathbf{n_s}$ are the

unknowns of the system. The development of the system of equations (2) and (3) is presented in greater detail in Appendix A. Each variable is expressed in complex notation, e.g., $\tilde{m} = m_1 + im_2$, and similarly for the other four variables, where the directions 1 and 2 refer to the two equatorial directions in either the mantle reference frame (for $\tilde{m}$, $\tilde{m}_f$, $\tilde{m}_s$, and $\tilde{n}_s$) or the ecliptic normal (for $\tilde{p}$). The external torque that drives the perturbations in rotation is periodic and proportional to $\exp[i\omega\Omega_o t]$, where ω is the frequency of the forcing expressed in cycles per lunar day and is equal to

$$\omega = -1 - \delta\omega\,, \tag{4}$$

where $\delta\omega = \Omega_p/\Omega_o$= 27.322 days/18.6 years = 4.022×10^{-3} is the Poincaré number, expressing the ratio of precession to rotation frequency. Small amplitudes are assumed, in which case $\tilde{p}$, $\tilde{m}$, $\tilde{m}_f$, $\tilde{m}_s$, and $\tilde{n}_s$ are equivalent to angles of misalignment and equations (2) and (3) can be cast into a linear system of five equations and five unknowns,

$$\mathrm{M} \cdot \mathbf{x} = \mathbf{y}\,, \tag{5}$$

where

$$\mathrm{M} = \begin{pmatrix} (1+\omega)(1+e)+\beta\Phi_2 & (1+\omega) & (1+\omega)\bar{A}_f/\bar{A} & (1+\omega)\bar{A}_s/\bar{A} & (1+\omega+\Phi_2)\alpha_3 e_s\bar{A}_s/\bar{A} \\ \beta\Phi_2 & \omega - e & (1+\omega)\bar{A}_f/\bar{A} & (1+\omega)\bar{A}_s/\bar{A} & (1+\omega+\Phi_2)\alpha_3 e_s\bar{A}_s/\bar{A} \\ 0 & \omega & 1+\omega+e_f+K_{\mathrm{icb}}\bar{A}_s/\bar{A}_f & -K_{\mathrm{icb}}\bar{A}_s/\bar{A}_f & -\omega\alpha_1 e_s\bar{A}_s/\bar{A}_f \\ \alpha_3 e_s\Phi_2 & \omega-\alpha_3 e_s & \alpha_1 e_s - K_{\mathrm{icb}} & 1+\omega+K_{\mathrm{icb}} & (1+\omega-\alpha_2+\alpha_3\Phi_2)e_s \\ 0 & 0 & 0 & 1 & \omega(1+i/(\omega\tau)) \end{pmatrix}, \tag{6a}$$

$$\mathbf{x} = \begin{pmatrix} \tilde{p} \\ \tilde{m} \\ \tilde{m}_f \\ \tilde{m}_s \\ \tilde{n}_s \end{pmatrix}, \mathbf{y} = \begin{pmatrix} -\beta\Phi_1 \\ -\beta\Phi_1 \\ 0 \\ -\alpha_3 e_s\Phi_1 \\ 0 \end{pmatrix}. \tag{6b}$$

The parameters that appear in this system include the dynamical ellipticities of the whole Moon (e), fluid core (e_f), and inner core (e_s) defined as

$$e = \frac{C-\bar{A}}{\bar{A}}\,, \qquad e_f = \frac{C_f-\bar{A}_f}{\bar{A}_f}\,, \qquad e_s = \frac{C_s-\bar{A}_s}{\bar{A}_s}\,, \tag{7}$$

where ($C > \bar{A}$), ($C_f > \bar{A}_f$), and ($C_s > \bar{A}_s$) are, respectively, the polar and mean equatorial moments of inertia of the whole Moon, fluid core, and inner core. The parameters α_1, α_2, α_3, and α_g depend on the interior density profile and capture the strength of pressure and gravitational coupling on the inner core. Formal definitions of these parameters are given in equations (A8) and (A14) of Appendix A; definitions for a model of homogeneous layers are given later in this section by equation (16). The parameter K_{icb} is a coupling constant that captures the strength of the electromagnetic torque at the ICB (see equation (A15) of Appendix A). The parameters Φ_1, Φ_2, and β capture the strength of the torque from Earth acting on the Moon. They involve the angle of the inclination of the Moon's orbit I and are defined by

$$\Phi_1 = \frac{3}{2}\frac{n^2}{\Omega_o^2}\frac{\cos(I)\sin(I)}{(1-e_L)^{3/2}}\,, \tag{8a}$$

$$\Phi_2 = \frac{3}{2}\frac{n^2}{\Omega_o^2}\frac{\left(\cos^2(I)-\sin^2(I)\right)}{(1-e_L)^{3/2}}\,, \tag{8b}$$

$$\beta = \frac{C-A}{B} \approx \frac{C-A}{\bar{A}} = e\left(1+2\frac{C_{22}}{J_2}\right)\,. \tag{8c}$$

Here A and B are the minimum and maximum equatorial moments of inertia of the whole Moon, J_2 and C_{22} are the unnormalized degree 2 coefficients of the Moon's gravity field, e_L is the orbit eccentricity, and n is the mean motion of the Moon, defined as

$$n^2 = \frac{G\left(M_E+M\right)}{a_L^3}\,, \tag{9}$$

where M_E and M are the masses of Earth and Moon, respectively, and a_L the semimajor axis radius of the Moon's orbit.

A couple of points are important to note about the system of equations (5) and (6). First, although we have developed our model under the assumption of an axially symmetric Moon, because of the synchronous rotation of the Moon around Earth, it is the minimum principal axis A that remains in alignment toward the Earth and the Moon is torqued about the principal axis B. So the amplitude of the torque, as reflected in the parameter β, involves the factor $(C - A)/B$. In the denominator of this factor, we have made the approximation $B \approx \bar{A}$, though we have kept A in the nominator. This leads to the term involving C_{22} in the amplitude of the prescribed torque, a term which of course should be zero for an axially symmetric Moon. However, although we consider the rotational response of an axisymmetric body, the amplitude of the torque is more accurately described by the inclusion of this C_{22} term, so we keep it in our model.

Second, the interior coupling part of the model was developed specifically to study Earth's nutations and as such assumes that all perturbations from uniform rotation are very small in amplitude. For the Moon, the perturbations in rotation can reach a few degrees of misalignment, as our results will show. Thus, although they remain small, they do not strictly satisfy the very small perturbation approximation and this introduces errors in accuracy. Near resonances, where misalignment angles can be larger than 10°, the accuracy of our model is expected to degrade significantly.

Third, we have neglected all elastic deformations in our derivation. Given the very small k_2 Love number of about 0.02 [*Williams et al.*, 2014b], our approximation of a rigid mantle should not introduce any significant error between our model and the real Moon. However, we must be careful when applying this model to other planets or moons for which elastic deformations may play a more significant role.

A fourth point concerns the mantle tilt angle ($\tilde{p}$). Lunar laser ranging gives us this tilt: $\theta_p = 1.543°$. We could have opted to use this value as a parameter for the prescription of the torque applied on the internal coupling system of equations (3) and simply monitor the internal response to this torque. However, leaving $\tilde{p}$ as a variable allows us to determine how it may be affected by coupling with the fluid and solid core. We will show that for the Moon, because the core is small, core-mantle coupling does not lead to a significant change in $\tilde{p}$. However, this may not be the case for other planets and moons for which a comparison between the observed mantle tilt and that predicted by equations (5) and (6) may then allow one to constrain interior models [e.g., *Baland et al.*, 2012]. We further note that $\tilde{p}$ and $\tilde{m}$ are tied by the following fundamental relationship: $\tilde{p} = -\tilde{m}/(1+\omega)$ [e.g., *Eckhardt*, 1981]. This connection between $\tilde{p}$ and $\tilde{m}$ is independent of the interior structure and composition of the Moon and can indeed be extracted from the first two equations of the system of equations (5) and (6) (see Appendix A, equations (A36) and (A37)).

The system of equations (5) and (6) contains five free modes which are determined by the eigensolutions of $\mathrm{M} \cdot \mathbf{x} = \mathbf{0}$. Four of these result from the internal coupling dynamics (equations (3)): these are the Chandler wobble, free core nutation (FCN), free inner core nutation (FICN), and inner core wobble [*Mathews et al.*, 1991a, 1991b]. The addition of equation (2) introduces one additional free mode: the free precession of the mantle tilt in space. The latter mode is a free precession in the sense that its angle of precession is arbitrary; its frequency depends on the gravitational potential imposed by Earth. The addition of equation (2) also introduces small modifications to the four free modes from internal coupling described by *Mathews et al.* [1991a, 1991b]. Likewise, the free precession of the mantle is also slightly altered by coupling with the fluid core and inner core. If the frequency of the forcing approaches that of the FCN or the FICN, resonant amplification can occur. These two modes are described in more detail in the next two subsections.

As a final note, we must point out that we have adopted an oversimplified representation of flow motion in the fluid core, restricted to a simple solid body rotation. In reality, the fluid core can sustain different types of waves which can interact with the free modes. In the context of our study, the most relevant are inertial waves, which have a frequency spectrum that overlaps that of the FCN and FICN. This means that the true FCN and FICN may be split into several modes covering a range of frequencies [*Rogister and Valette*, 2009].

2.4. The FCN and the Precession of the Fluid Core

The FCN describes the free precession motion of the axis of rotation of the fluid core when the latter is displaced from an alignment with the symmetry axis of the mantle ($\hat{\mathbf{e}}_3^{\mathbf{p}}$). The restoring force that sustains the oscillation is the pressure torque that the misaligned rotation vector of the core exerts on the elliptical

surface of the CMB. A good approximation of the FCN frequency, when expressed in cycles per rotation period in a frame fixed in inertial space, is

$$\omega_{\text{fcn}} \approx -e_f \frac{\bar{A}}{\bar{A}_m}\,, \tag{10}$$

where $\bar{A}_m = \bar{A} - \bar{A}_f - \bar{A}_s$ is the mean equatorial moment of inertia of the mantle. In the frame attached to the rotating mantle, the FCN frequency is $\omega_{\text{fcn}} = -1 - e_f\bar{A}/\bar{A}_m$. Note that the FCN is negative, implying that its direction of motion is retrograde.

The period of the FCN gives the timescale by which the fluid core can adjust to a change in the orientation of the mantle. For a small core, $\bar{A}/\bar{A}_m \approx 1$, and taking the dynamical ellipticity of the fluid core to be the same as that of the whole Moon, $e_f = 5.18{\cdot}10^{-4}$, gives an estimate of the FCN frequency for the Moon of $-1.38{\cdot}10^{-9}$ s^{-1} (in a space-fixed frame), or a period of $\sim$ 145 years, similar to the value computed in *Gusev and Petrova* [2008]. Because the ellipticity of the fluid core is likely smaller than that of the whole Moon, the FCN period should be longer than this simple estimate. Regardless of its exact value, since the retrograde rate of precession of the lunar mantle (frequency $\Omega_p = -2\pi/18.6$ yr^{-1} $= -1.07 \cdot 10^{-8}$ s^{-1}) is much faster than the FCN, the fluid core should be only weakly entrained by the precessing mantle [*Goldreich*, 1967; *Meyer and Wisdom*, 2011].

2.5. The FICN and the Precession of the Inner Core

The FICN describes the free precession motion of the combined rotation and symmetry axes of the inner core when they are offset from $\hat{\mathbf{e}}_3^{\mathbf{p}}$. As is the case for the FCN, the fluid pressure acting on the elliptical shape of the ICB contributes to the restoring force that maintains the oscillation. In addition, gravitational forces on the tilted elliptical inner core (as well as electromagnetic forces, if present) also contribute and it is the sum of these contributions that determines the frequency of the FICN. A good approximation of the FICN frequency, neglecting viscous deformation within the inner core, is

$$\omega_{\text{ficn}} \approx \left(e_s\alpha_2 - K_{\text{icb}} - e_s\alpha_3\Phi_2\right)\,, \tag{11}$$

when expressed in cycles per rotation period, in a frame fixed with inertial space. In a frame attached to the rotating mantle, the FICN frequency is $-1 + (e_s\alpha_2 - K_{\text{icb}} - e_s\alpha_3\Phi_2)$.

The FICN frequency involves the factor $\alpha_2 = \alpha_1 - \alpha_3\alpha_g$, which incorporates the pressure and gravitational torque from the rest of the Moon acting on a tilted solid core (exact definitions for these coefficients are given in equations (A8) and (A14) in Appendix A). The α_1 part captures the pressure torque from the misaligned rotation vector and the $\alpha_3\alpha_g$ term the gravitational torque (which includes its pressure contribution at the ICB) on the tilted figure of the solid core by the fluid core and mantle. The term $e_s\alpha_3\Phi_2$ accounts for the gravitational pull of the Earth on the tilted inner core. By itself, this latter term describes the free precession about the ecliptic normal of a tilted inner core in the Earth's gravitational potential. Because the gravitational pull from the mantle and fluid core is much greater than that from Earth, this term is a small correction to the FICN frequency of the Moon.

The FICN can be prograde or retrograde, depending on the relative strength between the pressure and gravitational torques. For Earth, based on the preliminary reference Earth model (PREM) [*Dziewonski and Anderson*, 1981], $\alpha_1 = 0.95$, $\alpha_3 = 0.05$, $\alpha_g = 2.18$ [*Mathews et al.*, 1991b], such that the pressure torque dominates and the FICN is prograde. (For this reason, it is referred to as the prograde free core nutation, or PFCN, in the studies of *Mathews et al.* [1991a, 1991b]). For typical models of the Moon interior, as we will show, we expect $\alpha_3\alpha_g \gg \alpha_1$, implying that the FICN is retrograde. Further, we will also show that by analogy with the period of the FCN, which gives the timescale at which the fluid core rotation axis can react to a change in the mantle orientation, the period of the FICN gives the timescale at which the inner core tilt switches from being driven by the exterior gravitational torque from Earth to being controlled by its gravitational coupling with the mantle.

2.6. A Simple Moon Model of Homogeneous Layers

For all calculations in this work, we use a simple four-layer model of the Moon with an external radius R, a solid inner core of radius r_s, a fluid core of radius r_f, a crust of thickness h_c, and a mantle with an outer radius of $r_m = R - h_c$. The densities of the solid inner core (ρ_s), fluid core (ρ_f), mantle (ρ_m), and crust (ρ_c) are assumed uniform. Adopting uniform density layers amounts to neglecting compressibility effects from increasing pressure with depth. Given the small pressures in the Moon's interior (less than about 5 GPa), this is certainly a good first-order description. The chief advantage of a uniform density layer model is that all the parameters that enter equations (5) and (6) can be expressed in analytical form, and we now proceed to describe how each is calculated and related to observational constraints.

2.6.1. Interior Mass Distribution of the Moon

We constrain our interior models of the Moon to be consistent with the observed bulk mass $M = (4\pi/3)\bar{\rho}R^3$, where $\bar{\rho}$ is the mean density. That is, for a model of homogenous density layers, we impose that

$$\bar{\rho}R^3 = \rho_s {r_s}^3 + \rho_f \left(r_f^3 - r_s^3\right) + \rho_m \left(r_m^3 - r_f^3\right) + \rho_c \left(R^3 - r_m^3\right) . \tag{12}$$

A measure of the moment of inertia of the solid Moon I_{sm} is given by [*Williams et al.*, 2014b]: $I_{\mathrm{sm}}/MR^2 = 0.393112 \pm 0.000012$ (the value appropriate for a reference radius of $R = 1737.151$ km). This value is based on the observed librations of the Moon. It involves the mantle and crust but may also involve the inner core if the latter follows the mantle by gravitational coupling. Because of its small size, the inner core contribution to I_{sm} is very small, and so for simplicity, we assume here that I_{sm} only contains the contribution from the mantle and crust. This gives a second constraint for our interior Moon models, namely, that the density of the mantle and crust must be consistent with I_{sm}, so

$$I_{\mathrm{sm}} = \frac{8\pi}{15}\left[\rho_m \left(r_m^5 - r_f^5\right) + \rho_c \left(R^5 - r_m^5\right)\right] . \tag{13}$$

To build an interior Moon model, the procedure that we follow is first to select the radii of the interior boundaries (r_s, r_f, and r_m). Then, we use $\rho_s = 7700$ kg m^{-3}, commensurate with the density of solid iron in face-centered cubic phase (γ-Fe) at pressures and temperatures expected at the center of the Moon [e.g., *Tsujino et al.*, 2013], and $\rho_c = 2550$ kg m^{-3}, the crustal density reported in *Wieczorek et al.* [2013]. The densities of the mantle and fluid core are then determined by matching the constraints on $\bar{\rho}$ and I_{sm} from equations (12) and (13).

2.6.2. Parameters of Our Rotational Model

For uniform density layers, the mean moments of inertia of the inner core, fluid core, and whole Moon are

$$I_s = \frac{8\pi}{15}\rho_s r_s^5 , \tag{14a}$$

$$I_f = \frac{8\pi}{15}\rho_f \left(r_f^5 - r_s^5\right) , \tag{14b}$$

$$I_M = \frac{8\pi}{15}\left[(\rho_s - \rho_f)r_s^5 + (\rho_f - \rho_m)r_f^5 + (\rho_m - \rho_c)r_m^5 + \rho_c R^5\right] . \tag{14c}$$

Once the radii and densities of each layer are known (determined as explained in the previous section), then I_s, I_f and I_M can be calculated. For convenience, we set $\bar{A}_s = I_s$, $\bar{A}_f = I_f$, and $\bar{A} = I_M$ in equations (5) and (6). Considering that ellipticities are smaller than 10^{-3}, this only entrains an error of the same order.

Equations (5) and (6) also require the dynamical ellipticities e, e_f, and e_s, which involve the polar and equatorial moments of inertia of each region. The latter depend on the interior density profile and on the degree 2 order 0 (i.e., pole-to-equator) topography at the boundaries of each region (exact definitions are given in equation (A5) in Appendix A). We characterize the pole-to-equator topography in terms of a flattening, defined as the difference between the equatorial and polar radius divided by the mean spherical radius. The flattening at the ICB, CMB, crust-mantle boundaries, and surface of the Moon are labeled, ϵ_s, ϵ_f, ϵ_m, and ϵ_r, respectively. The difference between the equatorial and polar radius at each of these interfaces is then $r_s\epsilon_s$, $r_f\epsilon_f$, $r_m\epsilon_m$, and $R\epsilon_r$, respectively. For uniform density layers, the dynamical ellipticities are related to the densities and flattenings by

$$e_s = \epsilon_s , \tag{15a}$$

$$e_f = \frac{r_f^5\epsilon_f - r_s^5\epsilon_s}{r_f^5 - r_s^5} , \tag{15b}$$

$$\begin{aligned} e &= \frac{(\rho_s - \rho_f)r_s^5\epsilon_s + (\rho_f - \rho_m)r_f^5\epsilon_f + (\rho_m - \rho_c)r_m^5\epsilon_m + \rho_c R^5\epsilon_r}{(\rho_s - \rho_f)r_s^5 + (\rho_f - \rho_m)r_f^5 + (\rho_m - \rho_c)r_m^5 + \rho_c R^5} , \\ &= \frac{8\pi}{15}\frac{1}{\bar{A}}\left[(\rho_s - \rho_f)r_s^5\epsilon_s + (\rho_f - \rho_m)r_f^5\epsilon_f + (\rho_m - \rho_c)r_m^5\epsilon_m + \rho_c R^5\epsilon_r\right] . \end{aligned} \tag{15c}$$

Numerical values for e, e_f, and e_s thus require knowledge of the flattening at the surface and at each of the interior boundaries. The latter are a priori unknown, though we explain in the next section how they are constrained by observations.

Finally, equations (5) and (6) also require the parameters $\alpha_1, \alpha_3, \alpha_2$, and α_g. Exact definitions of these parameters are given in Appendix A in equations (A8) and (A14). For uniform density layers, they are given by

$$\alpha_1 = \frac{\rho_f}{\rho_s}, \tag{16a}$$

$$\alpha_3 = 1 - \frac{\rho_f}{\rho_s}, \tag{16b}$$

$$\alpha_2 = \alpha_1 - \alpha_3 \alpha_g, \tag{16c}$$

$$\alpha_g = \frac{8\pi G}{5\Omega_o^2}\left[\rho_c(\epsilon_r - \epsilon_m) + \rho_m(\epsilon_m - \epsilon_f) + \rho_f \epsilon_f\right], \tag{16d}$$

where G is the gravitational constant.

2.6.3. The Elliptical Shape of the Moon

The parameters e_s, e_f, e, and α_g require knowledge of the flattening at the surface of the Moon and at each interior boundary. We use the observed topography of degree 2 order 0 at the surface of the Moon as given by *Araki et al.* [2009] which, for our choice of normalization, gives a surface flattening of $\epsilon_r = 1.2899 \times 10^{-3}$. The flattening at the crust-mantle boundary ϵ_m is not known. We specify ϵ_m so that it is consistent with the observed J_2 which, for homogeneous density layers, is given by

$$J_2 = \frac{8\pi}{15}\frac{1}{MR^2}\left[(\rho_s - \rho_f) r_s^5 \epsilon_s + (\rho_f - \rho_m) r_f^5 \epsilon_f + (\rho_m - \rho_c) r_m^5 \epsilon_m + \rho_c R^5 \epsilon_r\right]. \tag{17}$$

The expression for J_2 involves ϵ_s and ϵ_f; either these can be chosen as free variables or they can be related to ϵ_r and ϵ_m as we now describe.

The mass anomalies associated with ϵ_r and ϵ_m induce a gravitational potential in the mantle and core. Because the ICB should correspond to a surface of constant temperature (equal to the melting temperature of iron), it should also coincide with a surface of constant pressure and density and be at hydrostatic equilibrium. The topography of the ICB should then match an equipotential surface, in which case, following *Veasey and Dumberry* [2011], the ICB flattening ϵ_s can be expressed as a function of ϵ_r, ϵ_m, and ϵ_f by

$$\epsilon_s = k_{sr}\epsilon_r + k_{\mathrm{sm}}\epsilon_m + k_{sf}\epsilon_f, \tag{18a}$$

where

$$k_{sr} = \frac{\rho_c}{\frac{2}{3}\rho_s + \rho_f}, \qquad k_{\mathrm{sm}} = \frac{\rho_m - \rho_c}{\frac{2}{3}\rho_s + \rho_f}, \qquad k_{sf} = \frac{\rho_f - \rho_m}{\frac{2}{3}\rho_s + \rho_f}. \tag{18b}$$

The CMB flattening, ϵ_f, is poorly constrained by lunar laser ranging observations [e.g., *Williams and Boggs*, 2015], but it is probable that it is also in a state of hydrostatic equilibrium given the high temperatures deep in the Moon. Assuming hydrostatic equilibrium, and adapting the methodology presented in *Veasey and Dumberry* [2011], ϵ_f can be expressed in terms of ϵ_r, ϵ_m and ϵ_s,

$$\epsilon_f = k_{fr}\epsilon_r + k_{fm}\epsilon_m + k_{fs}\epsilon_s, \tag{19a}$$

where

$$k_{fr} = \frac{\rho_c}{\mathcal{P}}, \qquad k_{fm} = \frac{\rho_m - \rho_c}{\mathcal{P}}, \qquad k_{fs} = \frac{\left(\frac{r_s}{r_f}\right)^5 (\rho_s - \rho_f)}{\mathcal{P}}, \tag{19b}$$

$$\mathcal{P} = \rho_m + \frac{2}{3}\rho_f + \frac{5}{3}\left(\frac{r_s}{r_f}\right)^3 (\rho_s - \rho_f). \tag{19c}$$

Table 1. Reference Parameters for the Moon[a]

Moon Parameter	Numerical Value
Rotation rate, Ω_o	2.6617×10^{-6} s^{-1}
Orbit precession rate, Ω_p	$2\pi/18.6$ yr^{-1}
Poincaré number, $\delta\omega = \Omega_p/\Omega_o$	4.022×10^{-3}
Mean planetary radius, R	1737.151 km
Mass, M	7.3463×10^{22} kg
Mean density, $\bar{\rho}$	3345.56 kg m^{-3}
Moment of inertia of solid Moon, I_{sm}	$0.393112 \cdot MR^2$
J_2	2.03504×10^{-4}
C_{22}	2.44828×10^{-5}
Surface flattening, ϵ_r	1.2899×10^{-3}

[a]The values of R, M, $\bar{\rho}$, I_{sm}, J_2, and C_{22} are taken from *Williams et al.* [2014b]. The values for the unnormalized potential coefficients J_2 and C_{22} include the permanent tide from synchronous rotation with Earth and are obtained after multiplying the reported values in *Williams et al.* [2014b] by a factor of 1.000978 to take into account our choice of using the mean planetary radius as the reference radius for our calculations instead of the reference radius of 1738 km used in the GRAIL-derived gravity field. The value of ϵ_r is taken from *Araki et al.* [2009] and converted to our choice of normalization.

Further assuming that ϵ_s is at hydrostatic equilibrium, by plugging equation (18) in equation (19), we can express ϵ_f purely in terms of ϵ_r and ϵ_m,

$$\epsilon_f = \left(\frac{k_{fr} + k_{fs}k_{sr}}{1 - k_{fs}k_{sf}}\right)\epsilon_r + \left(\frac{k_{fm} + k_{fs}k_{sm}}{1 - k_{fs}k_{sf}}\right)\epsilon_m \,. \tag{20}$$

For a given interior model with radii and densities of each region specified, the coefficients k_{sr}, k_{sm}, k_{sf}, k_{fr}, k_{fm}, and k_{fs} can be readily calculated.

Note that in the derivation of equations (18a) and (19a) we have neglected a possible contribution from mass anomalies within the mantle. We have also neglected the gravitational tidal potential of the Earth and the centrifugal potential of the Moon's rotation, which are small compared to that from the mass anomalies induced by ϵ_r and ϵ_m. Since the observed flattening of the Moon through J_2 [*Williams et al.*, 2014b] is much larger than the expected tidal and rotational flattening [e.g., *Meyer and Wisdom*, 2011; *Le Bars et al.*, 2011], including these potentials would only introduce a small correction to our computed hydrostatic shapes. However, they were relatively more important in the past, when the Moon was both closer to Earth and rotating at a faster rate and so would need to be included in an investigation pertaining to the past Moon.

3. Results

3.1. Forced Precession of the Solid Core and Its Relation to the FICN

Our objective in this section is to illustrate a few general principles for the forced precession of the inner core of a planetary body. We use model parameters that are appropriate for the Moon, but the principles that we demonstrate are general and can be applied to the precession motion of any planet or satellite.

All the parameters that enter equations (5) and (6) can be readily calculated for a given choice of Ω_o, ω, R, r_s, r_f, h_c, ρ_s, ρ_f, ρ_m, ϵ_s, ϵ_f, ϵ_m, and ϵ_r. Some of these are directly observable and are listed in Table 1. For the crust, we assume a density of $\rho_c = 2550$ kg m^{-3} and a thickness of $h_c = 38.5$ km, which is the midpoint of the range of 34 to 43 km reported in *Wieczorek et al.* [2013]. We take $r_f = 350$ km, consistent with inferences from seismic studies [*Weber et al.*, 2011; *Garcia et al.*, 2011]. For the inner core parameters, we pick a radius of $r_s = 200$ km and $\rho_s = 7700$ kg m^{-3} [e.g., *Tsujino et al.*, 2013]. Matching the mean density and the moment of inertia of the solid Moon ($\bar{\rho}$ and I_{sm}) determines the density of the mantle and fluid core: for this specific model, $\rho_m = 3376.7$ kg m^{-3} and $\rho_f = 5783.2$ kg m^{-3}. We use a surface flattening of $\epsilon_r = 1.2899 \times 10^{-3}$ [*Araki et al.*, 2009] and pick the flattening of the crust-mantle interface to be $\epsilon_m = -2.1475 \times 10^{-3}$ so that the degree 2 mass anomaly

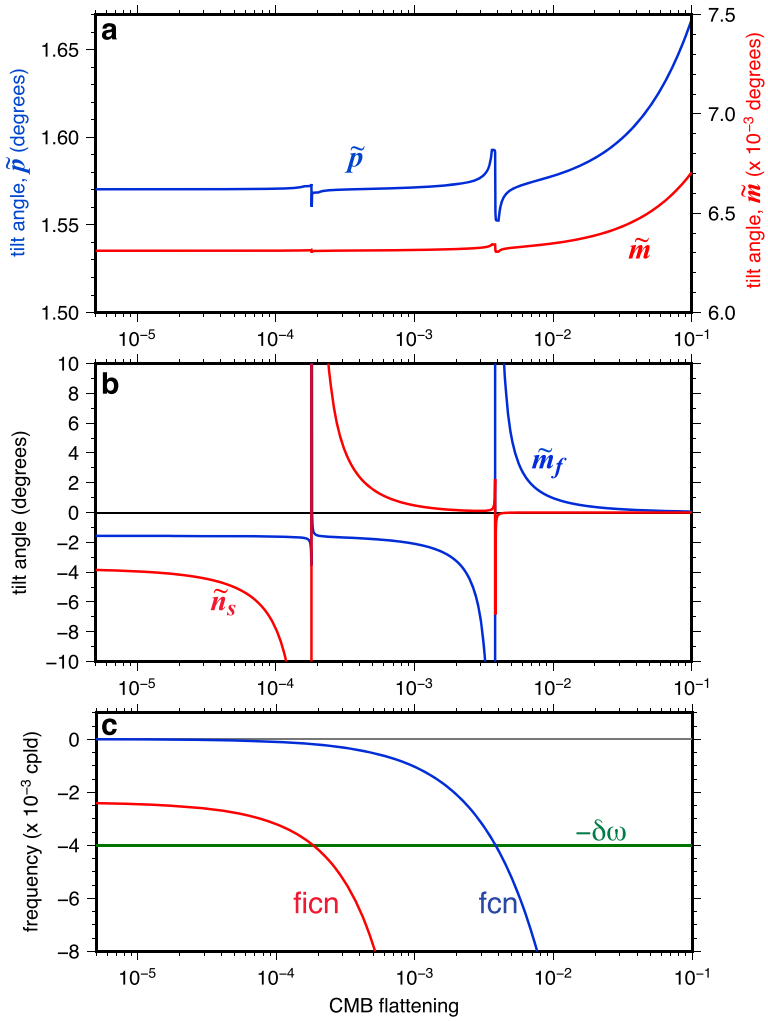

Figure 2. (a) Tilt angle of the mantle symmetry axis with respect to the ecliptic normal ($\tilde{p}$; blue, left axis) and tilt angle of the mantle rotation axis with respect to the mantle symmetry axis ($\tilde{m}$; red, right axis). (b) Tilt angle of the fluid core rotation axis $\tilde{m}_f$ (blue) with respect to the mantle rotation and tilt angle of the inner core symmetry axis $\tilde{n}_s$ (red) with respect to the mantle symmetry axis. (c) Frequency in cycles per lunar day (cpld) of the FICN (red), FCN (blue), and forcing frequency of the precession (green). Results show variations as a function of the CMB flattening (other parameters specified in the text).

from ϵ_r and ϵ_m alone (i.e., with no contribution from ϵ_s and ϵ_f) is compatible with J_2. Note that the negative flattening at the crust-mantle interface implies a partly isostatically compensated crust.

With $\epsilon_f = \epsilon_s = 0$, the FCN and FICN modes do not exist. To illustrate how the precession dynamics is connected to the FCN and FICN frequency, we consider synthetic Moon models where ϵ_f is varied between 3×10^{-6} and 10^{-1} and then calculate ϵ_s from equation (18a) assuming that the inner core is in hydrostatic equilibrium. We emphasize that this range of ϵ_f is used here solely for the purpose of demonstrating how the precession dynamics is linked to the FCN and FICN of a planetary body. Both the lower end and the higher end of this range are unrealistic for the Moon as we expect ϵ_f should be approximately 2×10^{-4} if the CMB is at hydrostatic equilibrium with the imposed gravity field arising from a nonhydrostatic lithosphere [e.g., *Meyer and Wisdom*, 2011]. Furthermore, with the added contribution from ϵ_f and ϵ_s, our models are incompatible with the observed J_2.

3.1.1. Rigid Inner Core, No Electromagnetic Coupling

Let us first present the case for a rigid inner core ($\tau \rightarrow \infty$) and without electromagnetic coupling at the ICB ($K_{\mathrm{icb}} = 0$). For this case, there is no dissipation, the response of the Moon is in phase with the applied torque, and all variables are purely real. Figures 2a and 2b show the tilt angle of the symmetry axis of the mantle with

respect to the ecliptic ($\tilde{p}$), as a function of ϵ_f. Also shown are the tilt angles of the rotation axis of the mantle ($\tilde{m}$) and the symmetry axis of the solid core ($\tilde{n}_s$), both with respect to the symmetry axis of the mantle, and the tilt angle of spin vector of the fluid core ($\tilde{m}_f$) with respect to that of the mantle. Figure 2c shows the frequency of the FCN and FICN as a function of ϵ_f.

A good test of our model is that it should recover the observed tilt of the mantle symmetry axis with the ecliptic normal of θ_p =1.543° for values of ϵ_f of the order of 10^{-4}, the expected flattening if the CMB were at hydrostatic equilibrium with the imposed gravity field from the nonhydrostatic lithosphere [e.g., *Meyer and Wisdom*, 2011]. Except at very close proximity to the resonance with the FICN frequency (see below), our model predicts $\theta_p \approx \tilde{p} = 1.5703°$. This is a difference of approximately 2% to the observed value, an adequate fit given the various assumptions we have made in the construction of our model (axial symmetry, no elastic deformation, small angles, linearization, etc.).

As shown in Figure 2a, the absolute value of $\tilde{m}$ is small, of the order of 0.0063°, indicating that the rotation vector of the mantle remains in close alignment with the mantle symmetry axis. The reason for the small amplitude of $\tilde{m}$ compared to that of $\tilde{p}$ is because they are tied by the relationship $\tilde{p} = -\tilde{m}/(1+\omega)$ (see Appendix A, equation (A37)). With $\omega = -1 - \delta\omega$, we then have $\tilde{p} = \tilde{m}/\delta\omega$, and because $\delta\omega = 4.022 \times 10^{-3}$, $|\tilde{m}| \ll |\tilde{p}|$.

Figure 2b shows large resonant amplifications for $\tilde{m}_f$ and $\tilde{n}_s$ for values of ϵ_f at which the precession frequency matches the FICN and the FCN frequencies. Let us first describe the changes in the rotation vector of the fluid core, $\tilde{m}_f$. For our smallest value of ϵ_f, $\tilde{m}_f$ is misaligned from the mantle spin axis by an angle −1.5821°. Since the mantle spin axis ($\tilde{p}+\tilde{m}$) is tilted by 1.5703° + 0.0063° = 1.5766° to the ecliptic normal, this means that the fluid core remains closely aligned with the ecliptic normal, offset only by −0.0055°; the fluid core is only very weakly entrained by the mantle precession. We note that even for $\epsilon_f = 0$ the fluid core is not fully decoupled from the mantle. This is because the fluid core is coupled to the inner core by a pressure torque at the ICB and the inner core is coupled gravitationally with the mantle. For increasing ϵ_f, the frequency of the retrograde FCN increases (Figure 2c); when the FCN frequency coincides with the forcing frequency, a resonance occurs, and in the absence of dissipation the amplitude of $\tilde{m}_f$ becomes large. For larger ϵ_f, on the right-hand side of this resonance in Figure 2, the FCN is faster than the rate of forced mantle precession; the rotation vector of the fluid core is locked to the figure axis of the mantle, and the two precess together. The entrainment of the fluid core is accompanied by an increase in the tilt of the mantle's symmetry and rotation axes.

Figure 2 illustrates the well-known fact established in previous studies, and reiterated above, that whether the rotation axis of the fluid core follows the mantle depends on the frequency of the FCN relative to that of the precessing mantle. However, while the FCN determines the transition between locking or decoupling, the fluid core is almost completely locked (almost fully decoupled) only when the FCN frequency is at least an order of magnitude larger or smaller than the forcing frequency. For a range of frequencies covering approximately 1 order of magnitude on either side of the FCN, the misalignment angle of the fluid core can be large.

Figure 2 further shows how the precession of the figure axis of the solid inner core ($\tilde{n}_s$) is connected to the FICN frequency. Note first that the FICN is negative, a consequence of the fact that $\alpha_3\alpha_g > \alpha_1$ and implying that the FICN is retrograde. In fact, for our choice of parameters, $\alpha_1 \approx 0.75$, $\alpha_3 \approx 0.25$, and $\alpha_g \approx 94$ for $\epsilon_f \approx 2 \times 10^{-4}$, and so $\alpha_3\alpha_g \gg \alpha_1$, indicating that the gravitational torque from the rest of the Moon on a tilted inner core is much larger than the pressure torque.

The amplitude of $\tilde{n}_s$ and its connection to the FICN frequency can be understood from the angular momentum equation of the inner core (fourth row of equation (6a)). First, notice that for $\omega = -1 - \delta\omega$ and $|\delta\omega| \ll 1$ the last row of equation (6a) implies that $\tilde{m}_s \approx \tilde{n}_s$ when $\tau \to \infty$, in other words, that the rotation and figure axis of the inner core are locked together. Using this in the fourth row of equation (6a), neglecting electromagnetic coupling and the small contribution from $\tilde{m}$, the tilt of the inner core is governed by

$$\left(\delta\omega + \omega_{\text{ficn}}\right)\tilde{n}_s = \alpha_3 e_s(\Phi_1 + \Phi_2\tilde{p}) + \alpha_1 e_s \tilde{m}_f\,, \tag{21}$$

where we have substituted the expression for the FICN frequency. The first term on the right-hand side represents the gravitational torque from Earth on the inner core, and the second term captures the pressure torque from the misaligned rotation vector of the fluid core. Equation (21) is the equivalent of a Cassini state for the

inner core. When $|\delta\omega| \gg |\omega_{\text{ficn}}|$, which corresponds to the left-hand side of the FICN resonance in Figure 2, the tilt of the inner core is given by

$$\tilde{n}_s \approx \delta\omega^{-1}\left[\alpha_3 e_s(\Phi_1 + \Phi_2\tilde{p}) + \alpha_1 e_s \tilde{m}_f\right] . \tag{22}$$

The precise value of $\tilde{n}_s$ depends on the balance between the gravitational torque from Earth and the pressure torque at the ICB, but it does not depend on gravitational coupling with the mantle. When $\delta\omega$ is far from the FCN resonance, the expression for $\tilde{n}_s$ can be further simplified by substituting $\tilde{m}_f \approx -\tilde{p}$ (for $|\delta\omega| \gg |\omega_{\text{fcn}}|$) or $\tilde{m}_f \approx 0$ (for $|\delta\omega| \ll |\omega_{\text{fcn}}|$). For our choice of parameters, $|\omega_{\text{ficn}}|$ remains of the same order of magnitude as $|\delta\omega|$ even for the smallest values of ϵ_f in Figure 2c: gravitational coupling with the mantle remains important, and the angle of misalignment of $\tilde{n}_s = -3.828°$ for the smallest values of ϵ_f corresponds to the equilibrium of equation (21) with $\tilde{m}_f \approx -\tilde{p}$ substituted in the last term.

When instead $|\delta\omega| \ll |\omega_{\text{ficn}}|$ in equation (21), which corresponds to the right-hand side of the FICN resonance in Figure 2, the inner core tilt angle obeys

$$\tilde{n}_s \approx \frac{\alpha_3(\Phi_1 + \Phi_2\tilde{p}) + \alpha_1\tilde{m}_f}{\alpha_1 - \alpha_3\alpha_g - \alpha_3\Phi_2} . \tag{23}$$

As above, the precise angle of misalignment depends on the gravitational torque from Earth and the pressure torque at the ICB. However, now it is also influenced by the gravitational torque from the mantle through α_g. For our choice of parameters, $|\alpha_3\alpha_g| \gg |\alpha_1|$ and $|\alpha_g| \gg |\Phi_2|$, so that the denominator of equation (23) can be approximated by $-\alpha_3\alpha_g$. Since $\alpha_g \gg 1$, $\tilde{n}_s$ is very small, as observed in Figure 2b: the inner core tilt angle is gravitationally locked into an alignment with the mantle. This close alignment with the mantle on the right-hand side of the FICN resonance is a consequence of our choice of parameters, which corresponds to a situation where the gravitational influence of the mantle (through α_g) is much larger than that from the external body (through Φ_2). This is expected to be the case for most planetary situations. In a scenario for which $\alpha_g \sim \Phi_2$, then based on equation (23), $\tilde{n}_s$ should be of the same order as $\tilde{p}$.

In summary, the FICN frequency marks the transition between an inner core precession that is driven by the gravitational torque from Earth to one which is gravitationally locked to the mantle. As we observed for the FCN above, the solid inner core is mostly locked (or decoupled) to the mantle only when the FICN frequency is at least an order of magnitude larger (or smaller) than the forcing frequency. When the FICN frequency is within 1 order of magnitude on either side of the forcing frequency, and in the absence of dissipation, large inner core tilt amplitudes can be generated by resonance. Note that the relative signs of ω_{ficn} and $\delta\omega$ are important for a resonance effect to occur: ω_{ficn} and $\delta\omega$ must be nearly equal in magnitude but of opposite sign to make their sum vanishingly small in equation (21). If ω_{ficn} and $\delta\omega$ have the same sign, the amplitude of inner core tilt would vary smoothly between the two limits of equations (22) and (23) without a spike in amplitude. Recall that we have defined $\delta\omega$ to be positive for a retrograde precession (see equation (4)): a resonance can occur when the FICN is also retrograde, which is the case for the Moon.

Before we conclude this section, we note that an amplification in both $\tilde{p}$ and $\tilde{m}$ is also observed at the FCN and FICN resonances. However, the changes in amplitude remain small, which needs an explanation. By adopting a small angle approximation in our model, when the FCN or FICN is precisely equal to ω, our solutions are singular and unbounded. Consequently, $\tilde{p}$ and $\tilde{m}$ are also unbounded. In reality, because torques involve a product of sine and cosine of a misalignment angle (see, e.g., equation (A23)), the maximum of this product is 0.5 which occurs at an angle of 45°. To reflect this, and to show how the amplitude of $\tilde{p}$ of the Moon may be affected close to a resonance, the curve for $\tilde{p}$ in Figure 2a is calculated based on the first row of equation (6a) but with values of all other variables capped at ± 0.5. We proceeded similarly to compute $\tilde{m}$. Though the resonances are clearly seen, the change in amplitude in $\tilde{p}$ and $\tilde{m}$ is relatively small because the moments of inertia of the fluid core and inner core are very small compared to that of the mantle. This shows that even if the present-day Moon were very close to the FICN resonance, this would not translate into a noticeable effect on the precession angle θ_p of the mantle.

3.1.2. Influence of Viscous Inner Core Deformation

We now investigate the effect of introducing viscous relaxation within the inner core such that its symmetry axis can relax to the imposed torque acting on it. With the introduction of dissipation, all variables of our system now have both a real and an imaginary part. Figure 3 shows how the real part of $\tilde{n}_s$ varies as a function of ϵ_f for different choices of the viscous relaxation timescale, τ. When τ is 10 lunar days, the results do not differ

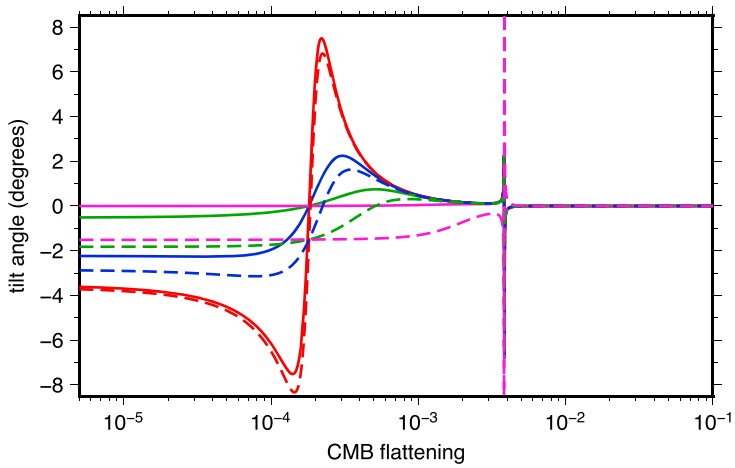

Figure 3. Tilt angle of the symmetry axis of the inner core (real part of $\tilde{n}_s$, solid lines) and tilt angle of the rotation axis of the inner core (real part of $\tilde{m}_s$, dashed lines) as a function of ϵ_f for different choices of the viscous relaxation timescale: (red) τ = 10 lunar days, (blue) τ = 3 lunar days, (green) τ = 1 lunar day, (purple) τ = 0.1 lunar day.

much from those in Figure 2b, except that the amplitude of $\tilde{n}_s$ remains finite at the FICN resonance. When τ is lowered further, the amplitude of $\tilde{n}_s$ near the FICN is more attenuated. If τ is of the order of 1 lunar day, the tilt angle is small even when $|\omega_{\text{ficn}}| < |\delta\omega|$. When the solid inner core has a much shorter relaxation timescale than its rotation period (e.g., $\tau = 0.1$ lunar day), the symmetry axis of the solid core remains aligned with that of the mantle.

Figure 3 shows that viscous relaxation of the Moon's inner core can have a significant impact on its misalignment angle. In the frame of the rotating mantle, a tilted inner core is seen as precessing with a period of 1 lunar day. This is why the relaxation timescale of the inner core must be of the order of one lunar day or less so that its shape can adjust significantly under the influence of the gravitational mantle torque. We also show in Figure 3 the angle of the rotation vector of the inner core, $\tilde{m}_s$. When $\tau \to \infty$, $\tilde{m}_s$ is almost perfectly aligned with $\tilde{n}_s$. But as τ is lowered, the two depart from one another, and for $\tau \to 0$, $\tilde{m}_s$ is aligned with the rotation axis of the fluid core.

3.1.3. Influence of Electromagnetic Coupling

The present-day Moon does not possess a core dynamo generating its own magnetic field, but paleomagnetic evidence suggests that one once existed in its past [e.g., *Weiss and Tikoo*, 2014]. If a radial magnetic field B_r threads the ICB, differential rotation between the fluid core and inner core leads to a shear of this field and to a resulting electromagnetic (EM) torque that acts to limit the differential rotation. To demonstrate the effect of EM coupling, we assume a uniform radial magnetic field of RMS strength $\langle B_r \rangle$. If we neglect the feedback from the Lorentz force on the fluid side of the boundary (weak field approximation), the coupling constant K_{icb} is related to $\langle B_r \rangle$ by [*Buffett*, 1992; *Buffett et al.*, 2002]

$$K_{\text{icb}} = -\frac{4\pi}{3}\frac{r_s^4 \langle B_r \rangle^2}{\Omega_o A_s}\gamma\left(\frac{\omega}{\|\omega\|} + i\right), \tag{24}$$

with

$$\gamma = \left(\frac{1}{\sigma_f \delta_f} + \frac{1}{\sigma_s \delta_s}\right)^{-1}. \tag{25}$$

Here σ_f and σ_s are the electrical conductivities and δ_f and δ_s are the magnetic skin depth, on the fluid and solid side of the ICB, respectively, which are given by

$$\delta_f = \sqrt{\frac{2}{\sigma_f \mu_o \Omega_o}}, \qquad \delta_s = \sqrt{\frac{2}{\sigma_s \mu_o \Omega_o}}, \tag{26}$$

where μ_o is the magnetic permeability of free space. In this weak field approximation, the amplitude of the coupling constant depends on the square of $\langle B_r \rangle$. However, when $\langle B_r \rangle$ is sufficiently large that the Lorentz

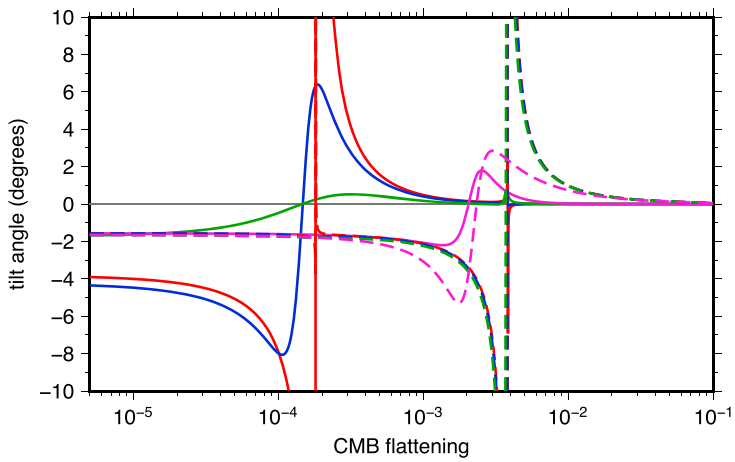

Figure 4. Tilt angle of the inner core (real part of $\tilde{n}_s$, solid lines) and the angle of the rotation axis of the fluid core (real part of $\tilde{m}_f$, dashed lines) as a function of ϵ_f for different choices of radial magnetic field at the ICB: $B_r = 0$ mT (red); $B_r = 0.04$ mT (blue); $B_r = 0.08$ mT (green); $B_r = 0.3$ mT (purple).

force can distort the flow in the fluid, the strength of the EM coupling becomes proportional to $\langle B_r \rangle$ [*Buffett et al.*, 2002; *Dumberry and Koot*, 2012], and the above model is no longer adequate. Nevertheless, we use here the weak field EM model given by equation (24) to provide a simple illustration of how the tilt angle of the inner core is affected by EM coupling.

EM coupling alters the results of Figure 2 in two ways. First, the real part of K_{icb} is positive, and therefore (see equation (11)) it shifts the FICN to a higher frequency in the retrograde direction. This is because, like gravitational coupling, EM coupling acts as a torque trying to reduce the misalignment of the inner core. Crossing of the FICN then occurs for smaller values of ϵ_f than in Figure 2b. Second, the shear of the radial magnetic field by the differential rotation at the ICB leads to ohmic dissipation, captured by the imaginary part of K_{icb}. This results in an attenuation and thus a reduction of the amplitude of $\tilde{n}_s$ near the FICN resonance.

Figure 4 shows how different values of $\langle B_r \rangle$ affect the real parts of $\tilde{n}_s$ and $\tilde{m}_f$. The chosen $\langle B_r \rangle$ values are not meant to be representative of the Moon's past; they are simply chosen here to illustrate the effect of EM coupling on the free modes. For these calculations, we have assumed $\sigma_f = \sigma_s = 1 \times 10^6$ S m^{-1}. For $\langle B_r \rangle = 0.04$ mT, the displacement of the FICN resonance and the attenuation of the solution can both be observed clearly. For a larger $\langle B_r \rangle$ of 0.08 mT, the amplitude of the inner core tilt near the FICN resonance is further attenuated. We also note that, contrary to attenuation from viscous deformation within the solid core, the attenuation from EM coupling does not result in an offset between $\tilde{m}_s$ and $\tilde{n}_s$: the real part of $\tilde{m}_s$ (not shown in Figure 4) remains almost aligned with the real part of $\tilde{n}_s$. This implies that if $\langle B_r \rangle$ is sufficiently large, EM coupling prevents a misalignment between $\tilde{n}_s$ and $\tilde{m}_f$. This is observed for $\langle B_r \rangle = 0.3$ mT, where the FICN resonance has disappeared completely. This further implies that EM coupling at the ICB also affects the solution near the FCN resonance; the entrainment of the inner core by the fluid core leads to a decrease in the retrograde FCN frequency, and ohmic dissipation attenuates the amplitude of all rotational variables. This is seen most clearly for $\langle B_r \rangle = 0.3$ mT.

3.2. Present-Day FICN Frequency and the Amplitude of the Inner Core Tilt

We now use our rotational model to investigate the range of possible FICN frequencies for the present-day Moon and the range of possible angles of the inner core tilt in its 18.6 year precession. We set $B_r = 0$, and as in the previous section, we take $h_c = 38.5$ km, $\rho_c = 2550$ kg m^{-3}, and $\rho_s = 7700$ kg m^{-3}. We assume an inner core radius of $r_s = 240$ km as suggested by a recent seismic model [*Weber et al.*, 2011], which is close to the maximum possible radius of 280 km inferred in *Williams et al.* [2014b]. We present results for r_f varying from 307 to 420 km, covering a range of outer core radii similar to that suggested by seismic studies [*Weber et al.*, 2011; *Garcia et al.*, 2011]. Matching $\bar{\rho}$ and I_{sm}, this translates into a range of fluid core densities ρ_f from 7459.1 to 4201.9 kg m^{-3} (for, respectively, $r_f = 307$ and 420 km) and so covers a broad range of possible light element concentrations in the fluid core and density jump at the ICB. The lower bound of $r_f = 307$ km is chosen such that ρ_f is compatible with the density of liquid iron at the Moon's core conditions, [e.g., *Tsujino et al.*, 2013]. The range of ρ_m is from 3376.1 to 3378.6 kg m^{-3}.

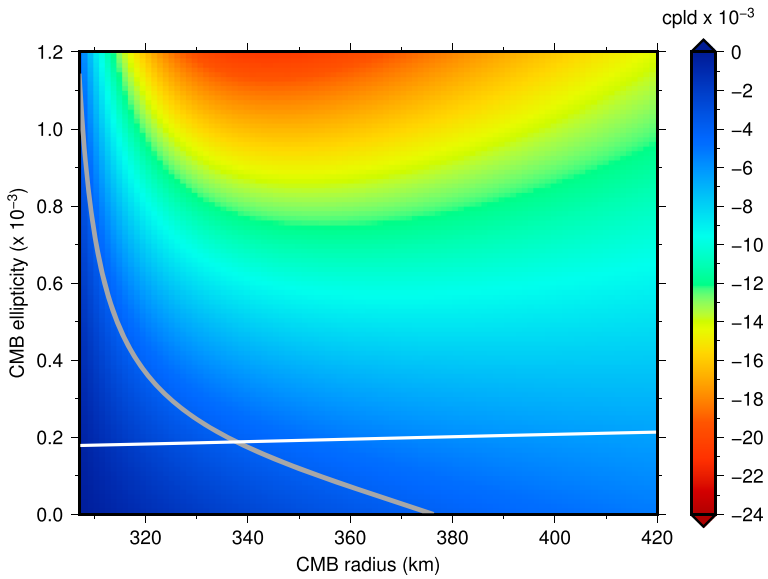

Figure 5. FICN frequency (color scale in cycles per lunar day, cpld) of the present-day Moon as a function of the fluid core radius r_f and CMB flattening ϵ_f. The calculation assumes a rigid inner core. The grey contour line marks the current location of the forcing frequency of the 18.6 year precession. The white line shows the value of ϵ_f as a function of r_f if the CMB is at hydrostatic equilibrium.

The FICN frequency depends on the flattening of the ICB, ϵ_s. If this interface is at hydrostatic equilibrium, then it relates to the flattening of the surface (ϵ_r), crust-mantle boundary (ϵ_m), and the CMB (ϵ_f) as given by equation (18). We take $\epsilon_r = 1.2899 \times 10^{-3}$. A CMB flattening of $\epsilon_f \sim 2.5 \times 10^{-4}$ has been inferred from physical librations measured by lunar laser ranging [*Williams et al.*, 2014b] though this value is poorly constrained [*Williams and Boggs*, 2015]. To show how the FICN frequency and the solid inner core tilt are influenced by ϵ_f (indirectly), we present results for a range of ϵ_f from 0 to 1.2×10^{-3}. Note that despite the uncertainty on ϵ_f, our upper bound is most likely too large. For each ϵ_f, the value of ϵ_m is then chosen by ensuring that the dynamical ellipticity of our model Moon is consistent with the observed J_2 coefficient of the gravitational potential (equation (17)).

Let us consider first a rigid inner core ($\tau \rightarrow \infty$). Figure 5 shows how the FICN, expressed in cycles per lunar day (cpld) in the space-fixed frame, of the present-day Moon varies as a function of the fluid core radius r_f and CMB flattening ϵ_f. The grey contour line in the figure marks the location of the forcing frequency of the 18.6 year precession, which equals -4.022×10^{-3} cpld. On the top right side of this grey line, the retrograde FICN frequency is faster than the rate of the forced precession, equivalent to being on the right-hand side of the resonance in Figure 2. Conversely, on the bottom left side of this grey line, the FICN frequency is slower, equivalent to being on the left-hand side of the resonance in Figure 2.

For the whole range of r_f and ϵ_f considered, Figure 5 shows that the FICN frequency is never too distant (i.e., by more than an order of magnitude) from the forcing frequency. This range can be narrowed if we focus on ϵ_f values that approach hydrostatic equilibrium. The white solid line in Figure 5 shows the value of ϵ_f as a function of r_f if the CMB is at hydrostatic equilibrium with mass anomalies induced by the flattenings ϵ_r, ϵ_m, and ϵ_s. In the vicinity of this hydrostatic equilibrium value, the FICN frequency never differs by more than a factor of 2 from the forcing frequency. That is, the FICN period (in a space-fixed frame) ranges from ~9 years to ~37 years.

Our computed FICN periods are very different from the values of 515 to 635 years reported by *Gusev and Petrova* [2008] based on the model of *Getino et al.* [1998]. We attribute this large difference to the fact that, as a cursory look of the expressions of the free modes given in *Getino et al.* [1998] reveal, their model fails to include properly the gravitational torque from the rest of the Moon acting on a tilted inner core.

The proximity of the FICN to the forcing frequency implies that the symmetry axis of the inner core is unlikely to be locked to the mantle and that, by a resonance effect, its angle of tilt is likely to be large. This is confirmed by Figure 6, which shows the amplitude of the tilt angle, $\tilde{n}_s$, for the same range of r_f and ϵ_f. If ϵ_f is near its

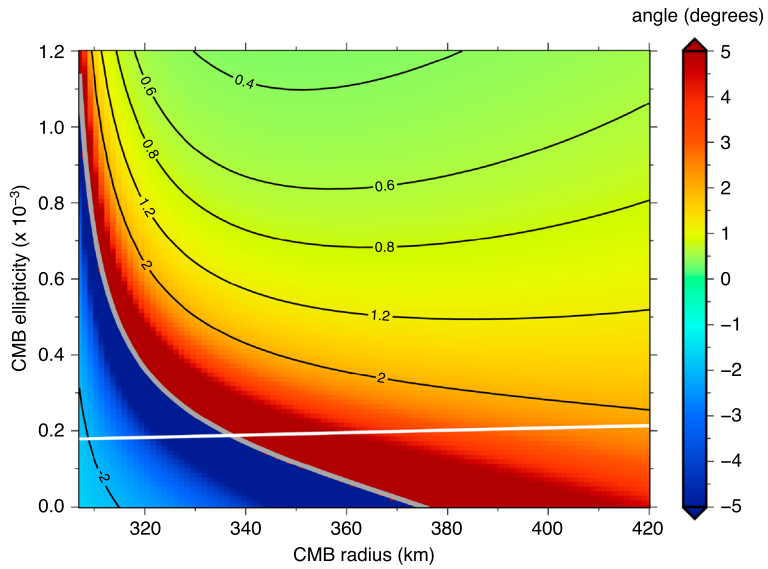

Figure 6. Amplitude of the tilt angle $\tilde{n}_s$ of a rigid inner core with respect to the mantle symmetry axis (color scale in degrees) of the present-day Moon as a function of the fluid core radius r_f and CMB flattening ϵ_f. Amplitudes have been saturated at ±5°. The location of the FICN resonance is indicated by the grey contour line. The white line shows the value of ϵ_f as a function of r_f if the CMB is at hydrostatic equilibrium. Selected contour lines are labeled to aid visualization.

hydrostatic equilibrium value, the absolute value of the inner core tilt angle is everywhere larger than 2°. In fact, it is even larger than 5° for a broad range of models with r_f between 320 and 360 km. We recall that large angles are incompatible with the small angle assumption of our rotational model, so the inner core tilt angles in Figure 6 have been truncated at a maximum angle of 5°. For a CMB flattening a few times larger than its hydrostatic value, the retrograde FICN frequency is larger and further away from resonance with the forcing frequency (except for models with $r_f < 320$ km); in this case the solid inner core tilt angle is mostly smaller than 1° (Figure 6).

Figure 7 shows the FCN frequency (in cpld in a space-fixed frame) as a function of the fluid core radius r_f and CMB flattening ϵ_f. The retrograde FCN frequency increases linearly with ϵ_f and is only weakly dependent

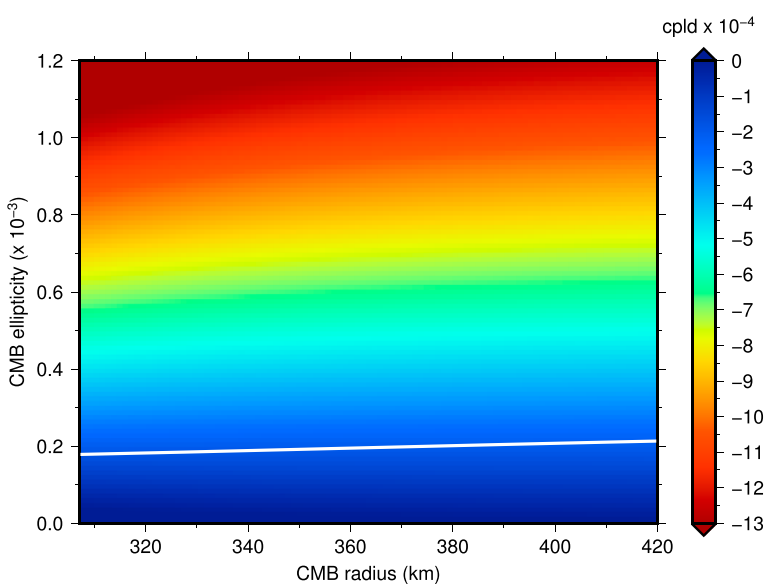

Figure 7. FCN frequency (color scale in cycles per lunar day, cpld) of the present-day Moon as a function of the fluid core radius r_f and CMB flattening ϵ_f. The calculation assumes a rigid inner core. The white line shows the value of ϵ_f as a function of r_f if the CMB is at hydrostatic equilibrium.

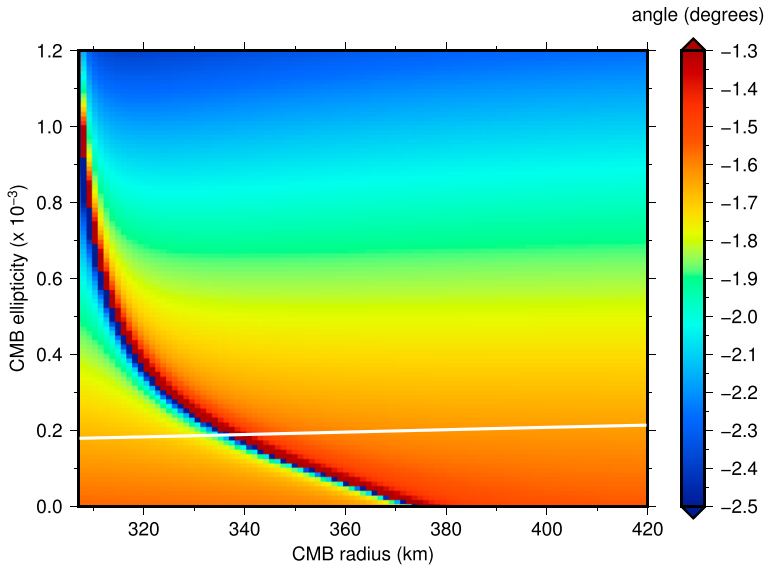

Figure 8. Amplitude of the tilt angle of spin axis of the fluid core $\tilde{m}_f$ with respect to the spin axis of the mantle (color scale, in degrees) of the present-day Moon as a function of the fluid core radius r_f and CMB flattening ϵ_f. The calculation assumes a rigid inner core. The white line shows the value of ϵ_f as a function of r_f if the CMB is at hydrostatic equilibrium.

on r_f. For ϵ_f values close to hydrostatic equilibrium, the FCN frequency is approximately -2×10^{-4} cpld. This corresponds to a FCN period (in a space-fixed frame) of approximately ~375 years. This is slightly longer, though similar, to the FCN period reported in *Gusev and Petrova* [2008] and *Williams et al.* [2014a].

Since the FCN frequency is smaller (in amplitude) by at least a factor of 10 than the forcing frequency of -4.022×10^{-3} cpld, the rotation vector of the fluid core in the present-day Moon should only be weakly entrained by the mantle precession. Indeed, as shown in Figure 8, for ϵ_f values close to hydrostatic equilibrium, $\tilde{m}_f$ takes values close to $-1.58°$ with respect to the spin vector of the mantle for most values of the fluid core radius. Our model predicts a tilt of the spin axis of the mantle by an angle ~1.57° with respect to the ecliptic. The misalignment of the spin vector of the fluid core with the ecliptic is then of the order of −0.01°. If ϵ_f is a few times larger than its hydrostatic value, the FCN frequency is increased (Figure 7), and because of its greater proximity to the forcing frequency, the amplitude of $\tilde{m}_f$ also increases and so does the pressure torque at the CMB. For our largest choice of $\epsilon_f = 1.2 \times 10^{-3}$, the coupling between the fluid core and the mantle is sufficiently important that $\tilde{m}_f \approx -2.3°$, corresponding to a misalignment of approximately −0.7° from the ecliptic normal. Figure 8 also reveals that, although $\tilde{m}_f$ does not depart much from the ecliptic normal if ϵ_f is close to its hydrostatic value, it can be excited to large amplitudes if the forcing frequency is very close to the FICN frequency. Though the resonance band is relatively narrow, it is clearly visible and is unsettlingly close to the 330 km fluid core radius value of *Weber et al.* [2011].

The results shown in Figures 5–8 pertain to a rigid inner core. Allowing the inner core to viscously relax introduces dissipation and, as we showed in section 3.1.2, it can lead to significant changes in the tilt angle of the solid inner core. Figure 9 shows how the real part of $\tilde{n}_s$ is affected when the viscous timescale τ is one lunar day. Although the very large angles at the resonance with the FICN are no longer present, the inner core tilt angles remain significant, of the same order as the tilt angle of the mantle with respect to the ecliptic normal. We also find that the large resonant amplitudes of $\tilde{m}_f$ in the narrow region around the FICN that we see in Figure 8 (where $\tau = \infty$) is no longer present when τ is one lunar day (not shown).

The results of Figures 5–9 do not change much for different choices of inner core radius than our adopted value of $r_s = 240$ km. Different values imply a different inner core mass and so a change in the mass balance of our interior models. For a given CMB radius r_f, a different combination of ρ_f and ρ_m is required to match $\bar{\rho}$ and I_{sm}. Therefore, the FICN and FCN frequencies as a function of r_f and ϵ_f are altered, which moves the location of the resonance curve in Figure 5. However, although the displacement of the FICN resonance also leads to a change in the amplitude of $\tilde{n}_s$ in Figure 6, the change is modest because the force balance that sets $\tilde{n}_s$ does not involve r_s directly but only the secondary effect that r_s has on other parameters (see equations (21)–(23)).

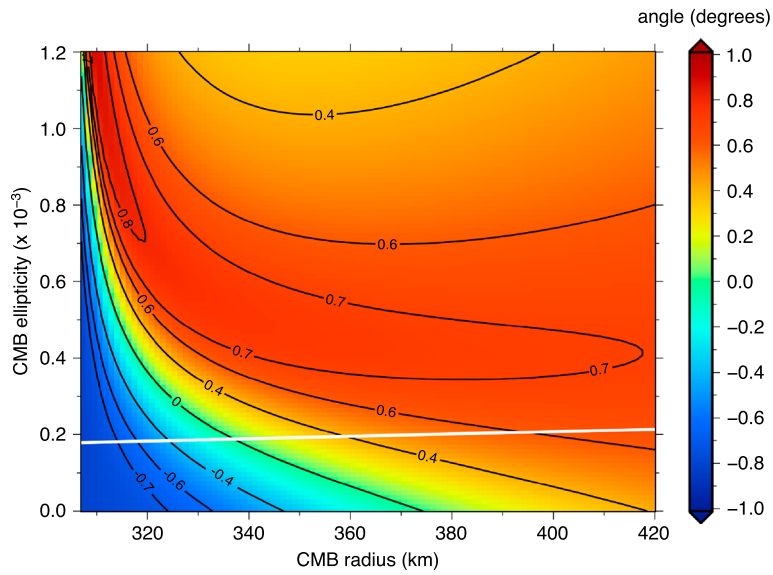

Figure 9. Real part of the tilt angle of the inner core $\tilde{n}_s$ with respect to the mantle symmetry axis (color scale, in degrees) of the present-day Moon as a function of the fluid core radius r_f and core-mantle flattening ϵ_f for an inner core with viscous relaxation time $\tau = 1$ lunar day. The white line shows the value of ϵ_f as a function of r_f if the CMB is at hydrostatic equilibrium. Selected contour lines are labeled to aid visualization.

Similarly, adopting a different crustal thickness than 38.5 km or a different crustal density than 2550 kg m^{-3} changes the overall mass balance but does not lead to substantial differences in the results we have presented above.

4. Discussion and Conclusion

We have shown in this work that the angle of precession of the solid inner core of a planetary body is determined to first order by its FICN frequency ω_{ficn}. The latter depends on the density structure of the core, including its elliptical shape. In a space-fixed reference frame, and expressed in cycles per rotation period, a good approximation of this frequency is $\omega_{\text{ficn}} \approx e_s\alpha_1 - e_s(1-\alpha_1)(\alpha_g + \Phi_2)$, when the inner core is assumed rigid and when viscous and electromagnetic coupling at the ICB play secondary roles. The parameters e_s and α_1 that enter this expression represent, respectively, the dynamical ellipticity of the inner core and the ratio of the fluid to solid density at the ICB. The parameters α_g and Φ_2 characterize the strength of the gravitational torque on the inner core by the mantle and an external body, respectively. The FICN frequency does not depend directly on the inner core radius r_s but only through the secondary effect that r_s has on e_s, α_1, and α_g.

The leading order torque balance that determines the inner core tilt depends on the relative amplitudes of ω_{ficn} and the forcing frequency $\delta\omega = \Omega_p/\Omega_o$, where Ω_p and Ω_o are the precession and rotation frequencies, respectively. If $|\omega_{\text{ficn}}| \ll |\delta\omega|$, the precession angle of the inner core is set by a balance between the pressure torque at the ICB (from the misaligned rotation vector of the fluid core) and the precession driving gravitational torque from the external body acting on its elliptical figure. In this case, the inner core is blind to the gravitational influence of the mantle. In contrast, if $|\omega_{\text{ficn}}| \gg |\delta\omega|$, the gravitational influence of the mantle plays a role, and when it dominates, the inner core is gravitationally locked to the mantle and is nearly aligned with it. If $|\omega_{\text{ficn}}| \approx |\delta\omega|$ and if the external driving torque is in the same direction as the FICN mode, large inner core tilt angles can result by resonant excitation.

We have applied our model to determine, to first order, the 18.6 year precession angle of the Moon's inner core. For the Moon, ω_{ficn} is negative; the FICN is a retrograde precession of the symmetry and rotation axes of the inner core with respect to the mantle figure. We have shown here that for a rigid inner core and a broad range of possible core density structures, the FICN frequency in the present-day Moon is to within a factor of 2 of the forcing frequency $\delta\omega = \Omega_p/\Omega_o$ = 27.322 days/18.6 years = 4.022×10^{-3}. That is, the period of the FICN (in a space-fixed frame) ranges from ~9 years to ~37 years and lies within the resonance band of the 18.6 year precession. Consequently, the figure axis of the inner core should not be aligned with the

mantle figure. Instead, we expect a substantial offset between the two. Our calculations suggest an inner core tilt angle offset in the range of 2° to 5° with respect to the mantle but possibly larger if the FICN period is very close to 18.6 years and if dissipation is weak.

One possible source of dissipation that we have explored is viscous relaxation of the inner core; if significant viscous relaxation occurs over a timescale of one lunar day, the large amplitudes at the resonance are suppressed and the inner core tilt angle that we predict is more modest, between 0 and 0.5°. The viscosity of the inner core of planets is not well constrained. But experimental results suggest that it could be low [*Gleason and Mao*, 2013]; a deformation timescale of one lunar day may not be unreasonable. Electromagnetic coupling at the ICB is another source of dissipation and, although not active at present, may have been important in the past, when the Moon had an active dynamo [e.g., *Weiss and Tikoo*, 2014]. Other possible sources of dissipation include turbulent viscous coupling at the CMB and ICB [e.g., *Yoder*, 1981; *Williams et al.*, 2001] and viscous relaxation in the lower mantle if the latter is partially molten [*Weber et al.*, 2011]. Our focus in this study has been on how dissipation affects the tilt angle of the inner core, but dissipation is also responsible for the observed lag of 0.26 arc sec of the mantle spin axis behind an exact Cassini state. Our model can be used to determine which of these dissipation mechanisms are compatible with this observational constraint.

A substantial misalignment between the precession angles of the inner core and mantle opens the possibility of detecting the former through gravity observations as suggested by *Williams* [2007]. In a frame of reference rotating with the mantle, the misaligned inner core traces a precession motion with a period of 27.212 days, which causes a periodic variation of the same period in the degree 2 and order 1 component of the lunar gravity field. An initial attempt to find this periodic inner core signal in the GRAIL data suggests that it is below noise level [*Williams et al.*, 2015]. If correct, the upper bound on the inner core gravity signal predicted on the basis of our model can thus be used as a constraint on the size, tilt angle, and rheology of the inner core, and also on the density contrast at the ICB. We plan to investigate this in more detail in a subsequent study.

It has been suggested that the Moon's past dynamo may have been sustained by a mechanical forcing from the differential rotation at the CMB [*Dwyer et al.*, 2011], when the tilt angle of the spin symmetry axis of the mantle with respect to the ecliptic was larger [*Ward*, 1975]. If this is correct, then differential rotation at the ICB can in principle also lead to dynamo action. Our model can be used to reconstruct the past history of the inner core tilt angle and therefore of the differential rotation at the ICB. Thus, our model can provide a basis for further investigations of a mechanical lunar dynamo.

Although the precise threshold criterion for dynamo action in these types of dynamos remains to be elucidated, it is most certainly connected to the amplitude of the differential velocity at the boundaries of the fluid core. As noted above, the proximity of the FICN period in the present-day Moon to the 18.6 year period of precession leads to a significant misalignment between the mantle spin symmetry axis and the inner core spin-symmetry axis. Our results have also shown that, for a FICN period very close to 18.6 years, a large misalignment of the spin axis of the fluid core with the mantle is also possible (Figure 8). If the past mechanical dynamo idea is correct, the differential rotation at the CMB and ICB in the present-day Moon must be below the threshold for dynamo action. In turn, this implies that the present-day FICN period cannot be too close to 18.6 years or that dissipation must limit the present-day differential rotation at the CMB and ICB. Either way, placing bounds on the differential rotation at the fluid core boundaries in connection to dynamo generation provides a path to extract constraints on the core of the Moon.

If the 18.6 year forcing is not at resonance with the FICN at present, could this resonance have been crossed at some point in the Moon's past? Or might it be crossed in the near future? To answer this, two factors are important. First, growth of a Fe-rich solid inner core changes the density of the fluid core over time (by enrichment of light elements) causing the FICN frequency to change. As an example of this, if we assume a core radius of $r_f = 340$ km and a fixed Poincaré number $\delta\omega$ equal to today's value, an inner core growth from 100 km to 240 km in radius would change the FICN period from being larger to smaller than 18.6 years, thus crossing the resonance. In the context of Figure 5, inner core growth results in the displacement of the resonance curve toward the lower left corner of the plot. A second way by which a resonance crossing may have occurred is by the evolution of the Earth-Moon orbital system and therefore a change in $\delta\omega$. As the semimajor axis of the lunar orbit expands with time, Ω_o decreases, and the amplitude of $\delta\omega$ increases. This causes the resonance curve in Figure 5 to be displaced toward the upper right corner with increasing time. For a fixed or very slowly evolving core density structure, interior models that are on the lower left side of the resonance in Figure 5

may have experienced a crossing in the past; those on the upper right side of it may experience a crossing in the future. To properly address this question, the time evolution of both $\delta\omega$ and the core density structure must be considered simultaneously.

Although the focus of our study has been on the Moon, many aspects of the solid inner core precession dynamics that we have illustrated here are general and can be applied to other planetary bodies. For instance, Mercury is also believed to be in a Cassini state [e.g., *Margot et al.*, 2012]. The forced precession of Mercury's orbit around the Sun is very slow, with its period being estimated at ~300,000 years. The measured J_2 of Mercury is smaller than that of the Moon, implying a smaller polar flattening and thus a slower FICN frequency. Nevertheless, we expect that the FICN frequency should be larger than the forced precession frequency by a couple orders of magnitude and, thus, that Mercury's inner core, if present, should be broadly aligned with the mantle axis. To do better justice to the Cassini state of Mercury's inner core and to predict its angle of tilt more precisely requires a more in-depth study. Indeed, a recent study suggests that gravitational coupling between the inner core and mantle may affect Mercury's Cassini state [*Peale et al.*, 2016].

Similarly, our model can also be applied to study the Cassini state of the icy satellites of Jupiter and Saturn. Like the Moon, these bodies are in synchronous rotation, though their precession dynamics is more complex because of the mutual gravitational influences between the satellites [*Bills*, 2005]. Their interiors are also characterized by a solid-liquid-solid structure, made up of an icy shell, a liquid ocean and a solid interior. The influence of the interior structure on the Cassini state of icy satellites has been investigated, for instance, in the study by *Baland et al.* [2012]. However, their model does not include the pressure torque arising from a misalignment of the rotation vector of the fluid layer with its solid boundaries. This pressure torque is a key ingredient of the FCN and FICN frequencies and, therefore, of the Cassini state of these icy satellites.

Finally, one can ask whether the inner core of Earth follows the mantle in its free precession of 26,000 years about the ecliptic normal. The FICN period for the Earth is prograde, and based on PREM it is predicted to be approximately 575 days [*Mathews et al.*, 1991b], though nutation observations suggest that it may be closer to ~930 days [*Koot et al.*, 2010], the difference being possibly accounted for by electromagnetic coupling at the ICB. Despite the uncertainty on its exact value, the FICN frequency is much shorter than the rate of mantle precession: the inner core should thus remain in close alignment with the mantle. As for Mercury above, a more focused study is required to obtain a precise value of the angle of tilt of the Earth's inner core 26,000 year precession.

Appendix A: A Model of the Rotational Dynamics of the Moon

A1. Internal Coupling Model

We assume an axisymmetric, rotating Moon of mean radius R composed of a mantle, a fluid outer core (radius r_f) and a solid inner core (radius r_s). We model the coupling between the Moon's interior regions by using the framework developed in *Mathews et al.* [1991a]. This model is described by the system of four equations given in the system of equation (3) of the main text, which we rewrite here for convenience,

$$\frac{\mathrm{d}}{\mathrm{d}t}\mathbf{H} + \mathbf{\Omega} \times \mathbf{H} = \mathbf{\Gamma}\,, \tag{A1a}$$

$$\frac{\mathrm{d}}{\mathrm{d}t}\mathbf{H_f} - \boldsymbol{\omega}_\mathbf{f} \times \mathbf{H_f} = -\mathbf{\Gamma_{icb}}\,, \tag{A1b}$$

$$\frac{\mathrm{d}}{\mathrm{d}t}\mathbf{H_s} + \mathbf{\Omega} \times \mathbf{H_s} = \mathbf{\Gamma_s} + \mathbf{\Gamma_{icb}}\,, \tag{A1c}$$

$$\frac{\mathrm{d}}{\mathrm{d}t}\mathbf{n_s} + \hat{\mathbf{e}}_\mathbf{3}^\mathbf{p} \times \left(\frac{\mathbf{n_s}}{\tau} + \boldsymbol{\omega}_\mathbf{s}\right) = \mathbf{0}\,. \tag{A1d}$$

The first three of these equations describe, respectively, the evolution of the angular momentum of the whole Moon ($\mathbf{H}$), the fluid core ($\mathbf{H_f}$), and solid inner core ($\mathbf{H_s}$). The fourth equation is a kinematic relation governing the tilt of the inner core relative to the mantle. The torques that appear on the right-hand side of these equations are the external torque from Earth ($\mathbf{\Gamma}$), the total gravitational and pressure torque exerted on a tilted inner core ($\mathbf{\Gamma_s}$), and the torque from viscous and electromagnetic surface tractions at the ICB ($\mathbf{\Gamma_{icb}}$).

These equations involve rotation vectors which are defined as follows. The reference equilibrium state is one of uniform rotation $\mathbf{\Omega}_o = \Omega_o \hat{\mathbf{e}}_\mathbf{3}^\mathbf{p}$ of all three regions with respect to a reference frame fixed to the symmetry

axis of the mantle, defined to be in the direction of unit vector $\hat{\mathbf{e}}_3^{\mathbf{p}}$. The external torque entrains changes in the orientation of the rotation vectors of the mantle ($\mathbf{\Omega}$), fluid core ($\mathbf{\Omega_f}$), and solid inner core ($\mathbf{\Omega_s}$). In the mantle frame, these are defined as

$$\mathbf{\Omega} = \mathbf{\Omega}_o + \boldsymbol{\omega}_{\mathbf{m}} = \Omega_o \left(\hat{\mathbf{e}}_3^{\mathbf{p}} + \mathbf{m}\right), \tag{A2a}$$

$$\mathbf{\Omega_f} = \mathbf{\Omega} + \boldsymbol{\omega}_{\mathbf{f}} = \Omega_o \left(\hat{\mathbf{e}}_3^{\mathbf{p}} + \mathbf{m} + \mathbf{m_f}\right), \tag{A2b}$$

$$\mathbf{\Omega_s} = \mathbf{\Omega} + \boldsymbol{\omega}_{\mathbf{s}} = \Omega_o \left(\hat{\mathbf{e}}_3^{\mathbf{p}} + \mathbf{m} + \mathbf{m_s}\right), \tag{A2c}$$

so that $\boldsymbol{\omega}_{\mathbf{m}} = \Omega_o \mathbf{m}$ describes the departure in mantle rotation with respect to $\hat{\mathbf{e}}_3^{\mathbf{p}}$, and $\boldsymbol{\omega}_{\mathbf{f}} = \Omega_o \mathbf{m_f}$ and $\boldsymbol{\omega}_{\mathbf{s}} = \Omega_o \mathbf{m_s}$ describe, respectively, the departure in the rotation of the fluid core and solid inner core with respect to $\mathbf{\Omega}$. The tilt of the inner core is defined as $\mathbf{n_s} = \hat{\mathbf{e}}_3^{\mathbf{s}} - \hat{\mathbf{e}}_3^{\mathbf{p}}$, the difference between the unit vectors $\hat{\mathbf{e}}_3^{\mathbf{s}}$ pointing in the direction of the symmetry axis of the inner core and $\hat{\mathbf{e}}_3^{\mathbf{p}}$. τ is the characteristic *e*-folding time of viscous relaxation of the inner core.

The angular momentum vectors $\mathbf{H}$, $\mathbf{H_f}$, and $\mathbf{H_s}$ are expanded as

$$\mathbf{H_s} = \mathcal{I}_{\mathbf{s}} \cdot \mathbf{\Omega_s}, \tag{A3a}$$

$$\mathbf{H_f} = \mathcal{I}_{\mathbf{f}} \cdot \mathbf{\Omega_f}, \tag{A3b}$$

$$\mathbf{H} = \mathcal{I} \cdot \mathbf{\Omega} + \mathcal{I}_{\mathbf{f}} \cdot \boldsymbol{\omega}_{\mathbf{f}} + \mathcal{I}_{\mathbf{s}} \cdot \boldsymbol{\omega}_{\mathbf{s}}, \tag{A3c}$$

where $\mathcal{I}_{\mathbf{s}}$, $\mathcal{I}_{\mathbf{f}}$, and $\mathcal{I}$ are the moment of inertia tensors of the solid inner core, fluid core, and the whole Moon, respectively. Explicit definitions of $\mathcal{I}_{\mathbf{s}}$, $\mathcal{I}_{\mathbf{f}}$, and $\mathcal{I}$ are given later in equation (A9). They involve the principal moments of inertia of the whole Moon ($C > B > A$), fluid core ($C_f > B_f > A_f$), and solid inner core ($C_s > B_s > A_s$). C, C_f, and C_s are the polar moments of inertia of each region, and since we assume axial symmetry, we need the mean equatorial moments of inertia of each region, defined as

$$\bar{A} = \frac{1}{2}(A + B) \qquad \bar{A}_f = \frac{1}{2}(A_f + B_f) \qquad \bar{A}_s = \frac{1}{2}(A_s + B_s). \tag{A4}$$

The polar and mean equatorial moments of inertia of the Moon are given, to the first order in pole-to-equator flattening ϵ, by

$$C = \frac{8\pi}{3} \int_0^R \rho \left(a'^4 + \frac{2}{15} \frac{\partial}{\partial a'} \left(a'^5 \epsilon\right)\right) \mathrm{d}a', \tag{A5a}$$

$$\bar{A} = \frac{8\pi}{3} \int_0^R \rho \left(a'^4 - \frac{1}{15} \frac{\partial}{\partial a'} \left(a'^5 \epsilon\right)\right) \mathrm{d}a'. \tag{A5b}$$

The moments of inertia of the inner core ($C_s, \bar{A}_s$) and fluid core ($C_f, \bar{A}_f$) are defined similarly by changing the lower and upper limits of integration in equation (A5) to, respectively, 0 to r_s and r_s to r_f. The flattening ϵ at a given radius defines the surface on which density is constant. ϵ is defined positive for an oblate spheroid, such that at a mean radius a the difference between the equatorial and polar radius is $a\epsilon$. The flattening at the ICB, CMB, crust-mantle boundaries, and surface of the Moon are labeled, ϵ_s, ϵ_f, ϵ_m, and ϵ_r, respectively.

The dynamical ellipticities of the whole Moon (e), fluid core (e_f), and solid inner core (e_s) are defined by

$$e = \frac{C - \bar{A}}{\bar{A}} \qquad e_f = \frac{C_f - \bar{A}_f}{\bar{A}_f} \qquad e_s = \frac{C_s - \bar{A}_s}{\bar{A}_s}. \tag{A6}$$

It is also convenient to define the principal moments of inertia C_s' and $\bar{A}_s'$ of a body of inner core shape but with uniform density ρ_{fs} equal to that on the fluid side of the ICB. The dynamical ellipticity of this body is

$$e_s' = \frac{C_s' - \bar{A}_s'}{\bar{A}_s'}, \tag{A7}$$

from which two more parameters are defined:

$$\alpha_1 = \frac{\bar{A}'_s e'_s}{\bar{A}_s e_s}\,, \tag{A8a}$$

$$\alpha_3 = 1 - \alpha_1 = 1 - \frac{\bar{A}'_s e'_s}{\bar{A}_s e_s}\,. \tag{A8b}$$

Neglecting elastic deformations, the moment of inertia tensors $\mathcal{I}_s$, $\mathcal{I}_\mathbf{f}$, and $\mathcal{I}$, in their instantaneous configurations, are expanded as [e.g., *Mathews et al.*, 1991a]

$$\mathcal{I}_\mathbf{s} = \bar{A}_s \mathbf{I} + \left(C_s - \bar{A}_s\right) \hat{\mathbf{e}}^\mathbf{s}_\mathbf{3} \hat{\mathbf{e}}^\mathbf{s}_\mathbf{3}\,, \tag{A9a}$$

$$\mathcal{I}_\mathbf{f} = \bar{A}_f \mathbf{I} + \left(C_f - \bar{A}_f\right) \hat{\mathbf{e}}^\mathbf{p}_\mathbf{3} \hat{\mathbf{e}}^\mathbf{p}_\mathbf{3} + \left(C'_s - \bar{A}'_s\right) \left(\hat{\mathbf{e}}^\mathbf{p}_\mathbf{3} \hat{\mathbf{e}}^\mathbf{p}_\mathbf{3} - \hat{\mathbf{e}}^\mathbf{s}_\mathbf{3} \hat{\mathbf{e}}^\mathbf{s}_3\right)\,, \tag{A9b}$$

$$\mathcal{I} = \bar{A}\mathbf{I} + \left(C - \bar{A}\right) \hat{\mathbf{e}}^\mathbf{p}_\mathbf{3} \hat{\mathbf{e}}^\mathbf{p}_\mathbf{3} + \left[\left(C_s - \bar{A}_s\right) - \left(C'_s - \bar{A}'_s\right)\right] \left(\hat{\mathbf{e}}^\mathbf{s}_\mathbf{3} \hat{\mathbf{e}}^\mathbf{s}_\mathbf{3} - \hat{\mathbf{e}}^\mathbf{p}_\mathbf{3} \hat{\mathbf{e}}^\mathbf{p}_\mathbf{3}\right)\,. \tag{A9c}$$

Here $\mathbf{I}$ is a unit tensor which leaves unchanged any vector on which it acts. These definitions are valid in any reference frame, provided $\mathbf{I}$ is defined as the unit tensor in the chosen frame (and $\hat{\mathbf{e}}^\mathbf{p}_\mathbf{3}$ and $\hat{\mathbf{e}}^\mathbf{s}_\mathbf{3}$ expanded in the vector components of this frame). In the mantle frame, $\mathbf{I} = \hat{\mathbf{e}}^\mathbf{p}_\mathbf{i} \hat{\mathbf{e}}^\mathbf{p}_\mathbf{j} \delta_{ij}$; in the ecliptic frame, $\mathbf{I} = \hat{\mathbf{e}}_\mathbf{i} \hat{\mathbf{e}}_\mathbf{j} \delta_{ij}$. Assuming small perturbations from uniform rotation (i.e., $\|\mathbf{m}\|$, $\|\mathbf{m_f}\|$, $\|\mathbf{m_s}\|$, and $\|\mathbf{n_s}\|$ are all $\ll 1$) the angular momentum vectors defined in equation (A3) are approximated as

$$\mathbf{H_s} = \Omega_o C_s \hat{\mathbf{e}}^\mathbf{p}_\mathbf{3} + \Omega_o \bar{A}_s (\mathbf{m} + \mathbf{m_s}) + \Omega_o \bar{A}_s e_s \mathbf{n_s}\,, \tag{A10a}$$

$$\mathbf{H_f} = \Omega_o C_f \hat{\mathbf{e}}^\mathbf{p}_\mathbf{3} + \Omega_o \bar{A}_f (\mathbf{m} + \mathbf{m_f}) - \Omega_o \bar{A}'_s e'_s \mathbf{n_s}\,, \tag{A10b}$$

$$\mathbf{H} = \Omega_o C \hat{\mathbf{e}}^\mathbf{p}_\mathbf{3} + \Omega_o \bar{A}\mathbf{m} + \Omega_o \bar{A}_f \mathbf{m_f} + \Omega_o \bar{A}_s \mathbf{m_s} + \Omega_o \bar{A}_s e_s \alpha_3 \mathbf{n_s}\,, \tag{A10c}$$

and the cross products on the left-hand side of equations (A1) are

$$\mathbf{\Omega} \times \mathbf{H_s} = \Omega_o^2 \hat{\mathbf{e}}^\mathbf{p}_\mathbf{3} \times \left[\bar{A}_s \mathbf{m_s} + \bar{A}_s e_s (\mathbf{n_s} - \mathbf{m})\right]\,, \tag{A11a}$$

$$\boldsymbol{\omega}_\mathbf{f} \times \mathbf{H_f} = \Omega_o^2 \hat{\mathbf{e}}^\mathbf{p}_\mathbf{3} \times \left[-C_f \mathbf{m_f}\right]\,, \tag{A11b}$$

$$\mathbf{\Omega} \times \mathbf{H} = \Omega_o^2 \hat{\mathbf{e}}^\mathbf{p}_\mathbf{3} \times \left[-Ae\mathbf{m} + \bar{A}_f \mathbf{m_f} + \bar{A}_s \mathbf{m_s} + \bar{A}_s e_s \alpha_3 \mathbf{n_s}\right]\,. \tag{A11c}$$

The four rotation variables $\mathbf{m}$, $\mathbf{m_f}$, $\mathbf{m_s}$, and $\mathbf{n_s}$ are the unknowns of the system. Each is expressed in complex notation, $\tilde{m} = m_1 + im_2$, and similarly for the other three variables, where the directions 1 and 2 refer to the two equatorial directions in the mantle reference frame. The cross product $\hat{\mathbf{e}}^\mathbf{p}_\mathbf{3} \times \mathbf{m}$ is replaced by $i\tilde{m}$, and similarly for the other three variables. For small amplitudes, they are equivalent to the angles of misalignment with respect to the symmetry axis of the mantle.

The external torque on the right-hand side of equation (A1) that drives the perturbations in rotation from the equilibrium state is expanded as

$$\tilde{\Gamma}(\omega) = \tilde{\Gamma} \exp[i\omega\Omega_o t]\,, \tag{A12a}$$

$$\tilde{\Gamma} = -i\bar{A}\Omega_o^2 \tilde{\phi}\,, \tag{A12b}$$

where $\tilde{\phi}$ specifies the amplitude of the external forcing at a given frequency ω, the latter being expressed in cycles per rotation period as seen from the rotating mantle frame. Note that our definition of $\tilde{\phi}$ differs by a factor of e from that used in *Mathews et al.* [1991a]. Any torque applied on the Moon can be decomposed in the frequency domain and expressed as a sum of terms of the form given by equation (A12). For small perturbations in rotation, the left-hand side of equations (A1) is linear in the four rotation variables, so that each term is also proportional to $\exp[i\omega\Omega_o t]$. Time derivatives are replaced by $i\omega\Omega_o$, and solutions can then be readily obtained in the frequency domain.

Our focus in this study is on the torque associated with the precession of the Moon's orbit. The torque applied on the figure of the Moon by the Earth can be approximated by taking the mean torque over one orbital period, with frequency $\omega = -1 - \delta\omega$, where $\delta\omega = \Omega_p/\Omega_o$= 27.322 days/18.6 years = 4.022×10^{-3} is the Poincaré number, expressing the ratio of precession to rotation frequency. The explicit expression for $\tilde{\phi}$, the amplitude of the mean torque, is deferred to the next section.

The gravitational and pressure torque exerted on a tilted inner core, Γ_s, when neglecting elastic deformations, is given by [*Mathews et al.*, 1991a]

$$\tilde{\Gamma}_s = i\Omega_o^2 \bar{A}_s e_s \left(-\alpha_1(\tilde{m} + \tilde{m}_f) + \alpha_2 \tilde{n}_s - \alpha_3 \tilde{\phi}_s\right) , \tag{A13}$$

where

$$\alpha_2 = \alpha_1 - \alpha_g \alpha_3 , \tag{A14a}$$

$$\alpha_g = \frac{8\pi G}{5\Omega_o^2} \left(\int_{r_s}^{R} \rho(a') \frac{\mathrm{d}\epsilon(a')}{\mathrm{d}a'} \mathrm{d}a' + \rho_{fs}\, \epsilon_s \right) . \tag{A14b}$$

The coefficient α_g captures the strength of gravitational coupling by the rest of the Moon on a tilted inner core, where G is the gravitational constant. The explicit definition of the external torque on the solid inner core, captured by $\tilde{\phi}_s$, is deferred to next section. $\mathbf{\Gamma_{icb}}$ is the torque from viscous and electromagnetic surface tractions acting on the solid inner core from differential rotation at the ICB. We neglect the torque from viscous forces here. The torque from electromagnetic (EM) forces can be important and is expressed in terms of a dimensionless coupling constant K_{icb} [*Buffett et al.*, 2002]

$$\tilde{\Gamma}_{\mathrm{icb}} = -i\Omega_o^2 \bar{A}_s (\tilde{m}_s - \tilde{m}_f) K_{\mathrm{icb}} . \tag{A15}$$

Regrouping all terms, the system of equations (A1) is written in the frequency domain as

$$(\omega - e)\tilde{m} + (1+\omega)\frac{\bar{A}_f}{\bar{A}}\tilde{m}_f + (1+\omega)\frac{\bar{A}_s}{\bar{A}}\tilde{m}_s + (1+\omega)\alpha_3 e_s \frac{\bar{A}_s}{\bar{A}}\tilde{n}_s = -\tilde{\phi} , \tag{A16a}$$

$$\omega\tilde{m} + \left(1 + \omega + e_f + K_{\mathrm{icb}}\frac{\bar{A}_s}{\bar{A}_f}\right)\tilde{m}_f - K_{\mathrm{icb}}\frac{\bar{A}_s}{\bar{A}_f}\tilde{m}_s - \omega\alpha_1 e_s \frac{\bar{A}_s}{\bar{A}_f}\tilde{n}_s = 0, \tag{A16b}$$

$$(\omega - \alpha_3 e_s)\tilde{m} + \left(\alpha_1 e_s - K_{\mathrm{icb}}\right)\tilde{m}_f + \left(1 + \omega + K_{\mathrm{icb}}\right)\tilde{m}_s + (1 + \omega - \alpha_2)e_s\tilde{n}_s = -\alpha_3 e_s \tilde{\phi}_s , \tag{A16c}$$

$$\tilde{m}_s + \omega\left(1 + \frac{i}{\omega\tau}\right)\tilde{n}_s = 0 . \tag{A16d}$$

A2. The Torque From Earth

Equation (2) of the main text determines the tilt of the symmetry axis of the mantle (i.e., orientation of the mantle frame) with respect to the ecliptic plane; we rewrite it here for convenience,

$$\frac{\mathrm{d}}{\mathrm{d}t}\mathbf{H} + \Omega_o \hat{\mathbf{e}}_3 \times \mathbf{H} = \mathbf{\Gamma} . \tag{A17}$$

The left-hand side of equation (A17) involves the angular momentum of the whole Moon, expressed in a frame rotating at angular velocity Ω_o that is aligned with the ecliptic normal $\hat{\mathbf{e}}_3$. We define the orientation of the mantle symmetry axis by $\hat{\mathbf{e}}_3^{\mathbf{p}} = \hat{\mathbf{e}}_3 + \mathbf{p}$. For $|\mathbf{p}| \ll 1$, $|\mathbf{p}|$ corresponds to the tilt angle of the symmetry axis of the mantle with respect to the ecliptic normal, which we define as θ_p . The rotation vector of the mantle as seen in the $\hat{\mathbf{e}}_3$ frame is

$$\mathbf{\Omega} = \Omega_o \left(\hat{\mathbf{e}}_3 + \mathbf{p} + \mathbf{m}\right) . \tag{A18}$$

The definitions given in equation (A9) are general and can be used to describe the moment of inertia tensors in the $\hat{\mathbf{e}}_3$ frame. Once again, if one assumes small perturbations from uniform rotation (i.e., $\|\mathbf{m}\|$, $\|\mathbf{m_f}\|$, $\|\mathbf{m_s}\|$, and $\|\mathbf{n_s}\|$ are all $\ll 1$) the angular momentum vector of the whole Moon is

$$\mathbf{H} = \Omega_o C(\hat{\mathbf{e}}_3 + \mathbf{p}) + \Omega_o \bar{A}\mathbf{m} + \Omega_o \bar{A}_f \mathbf{m_f} + \Omega_o \bar{A}_s \mathbf{m_s} + \Omega_o \bar{A}_s e_s \alpha_3 \mathbf{n_s} , \tag{A19}$$

and the cross product on the left side of equation (A17) is

$$\Omega_o \hat{\mathbf{e}}_3 \times \mathbf{H} = \Omega_o^2 \hat{\mathbf{e}}_3 \times \left[C\mathbf{p} + A\mathbf{m} + \bar{A}_f \mathbf{m_f} + \bar{A}_s \mathbf{m_s} + \bar{A}_s e_s \alpha_3 \mathbf{n_s} \right] . \tag{A20}$$

We proceed as for the interior coupling model and express $\mathbf{p}$ in complex notation, $\tilde{p} = p_1 + ip_2$. Directions 1 and 2 are the two equatorial directions in the $\hat{\mathbf{e}}_3$ frame, chosen to be aligned with the projection of the directions 1 and 2 of the $\hat{\mathbf{e}}_3^{\mathbf{p}}$ frame onto the $\hat{\mathbf{e}}_3$ frame. For a small tilt angle between $\hat{\mathbf{e}}_3^{\mathbf{p}}$ and $\hat{\mathbf{e}}_3$,

$$\hat{\mathbf{e}}_3 \times \mathbf{m} \approx \hat{\mathbf{e}}_3^{\mathbf{p}} \times \mathbf{m} \rightarrow i\tilde{m} , \tag{A21}$$

and similarly for $\mathbf{m_f}$, $\mathbf{m_s}$, and $\mathbf{n_s}$. Assuming again that each term is proportional to $\exp\left[i\omega\Omega_o t\right]$, and using $C = \bar{A}(1+e)$, the left-hand side of equation (A17) is

$$\frac{\mathrm{d}}{\mathrm{d}t}\mathbf{H} + \Omega_o \hat{\mathbf{e}}_3 \times \mathbf{H} \rightarrow i\Omega_o^2 (1+\omega) \left[\bar{A}(1+e)\tilde{p} + \bar{A}\tilde{m} + \bar{A}_f \tilde{m}_f + \bar{A}_s \tilde{m}_s + \bar{A}_s e_s \alpha_3 \tilde{n}_s \right] . \tag{A22}$$

The right-hand side of equation (A17) is the gravitational torque from Earth, which we now develop. Our focus is on the torque associated with the precession of the Moon's orbit. The amplitude of the torque applied on the figure of the Moon by the Earth can be approximated by taking the mean torque over one orbital period. Adopting our complex notation, this torque is proportional to $\exp\left[i\omega\Omega_o t\right]$, and if the Moon were a single, rigid body, its amplitude would be

$$\tilde{\Gamma} = -i\frac{3}{2}\frac{n^2}{(1-e_L)^{3/2}}(C-A)\sin(I+\theta_p)\cos(I+\theta_p) , \tag{A23}$$

where e_L is the orbit eccentricity, n is the mean motion of the Moon, with

$$n^2 = \frac{G\left(M_E + M\right)}{a_L^3} , \tag{A24}$$

where M_E and M are the masses of Earth and Moon, respectively, and a_L the semimajor axis radius of the Moon's orbit. Note that although we have developed our model under the assumption of an axially symmetric Moon, because of the synchronous rotation of the Moon around Earth, it is the principal axis associated with the minimum moment of inertia A that remains in alignment toward the Earth. Leaving A in equation (A23) instead of $\bar{A}$ gives slightly more accurate amplitude of the torque.

In the absence of an inner core, the torque given in equation (A23) is also valid for a Moon that comprises a fluid core. This is because the fluid trapped by the elliptical shape of the CMB is the only core contribution to $C-A$ for a uniform density core. For a radially varying density, there is an additional core contribution to $C-A$ from the elliptical equipotential surfaces within the fluid core, but they too follow the mantle because they deform to align with the imposed gravity field of the mantle.

For a Moon that comprises an inner core, tilted at an angle θ_s with respect to the mantle tilt θ_p, the torque acting on the whole of the Moon is

$$\begin{aligned}\tilde{\Gamma} = &-i\frac{3}{2}\frac{n^2}{(1-e_L)^{3/2}}\left[(C-A) - \bar{A}_s e_s \alpha_3\right]\sin(I+\theta_p)\cos(I+\theta_p) \\ &- i\frac{3}{2}\frac{n^2}{(1-e_L)^{3/2}}\left[\bar{A}_s e_s \alpha_3\right]\sin(I+\theta_p+\theta_s)\cos(I+\theta_p+\theta_s) ,\end{aligned} \tag{A25}$$

where, for simplicity, we have assumed that the torque on the inner core is proportional to $\bar{A}_s$, not A_s. Assuming small tilt angles, we substitute $\theta_p \approx \tilde{p}$ and $\theta_s \approx \tilde{n}_s$, and we use the following approximations:

$$\sin(I+\theta_p)\cos(I+\theta_p) \approx \cos I \sin I + \left(\cos^2 I - \sin^2 I\right)\tilde{p} , \tag{A26a}$$

$$\sin(I+\theta_p+\theta_s)\cos(I+\theta_p+\theta_s) \approx \cos I \sin I + \left(\cos^2 I - \sin^2 I\right)\left(\tilde{p} + \tilde{n}_s\right) . \tag{A26b}$$

Thus, the torque can be expanded as

$$\tilde{\Gamma} = -i\Omega_o^2 \bar{A}\tilde{\phi} , \tag{A27}$$

where

$$\tilde{\phi} = \beta\Phi_1 + \beta\Phi_2\tilde{p} + \frac{\bar{A}_s}{\bar{A}} e_s \alpha_3 \Phi_2 \tilde{n}_s \,, \tag{A28}$$

and where we have defined

$$\Phi_1 = \frac{3}{2}\frac{n^2}{\Omega_o^2}\frac{\cos I \sin I}{(1-e_L)^{3/2}} \,, \tag{A29a}$$

$$\Phi_2 = \frac{3}{2}\frac{n^2}{\Omega_o^2}\frac{\left(\cos^2 I - \sin^2 I\right)}{(1-e_L)^{3/2}} \,, \tag{A29b}$$

and

$$\beta = \frac{C-A}{B} \approx \frac{C-A}{\bar{A}} \,. \tag{A30a}$$

This approximated expression for β can also be written as

$$\beta = e\left(1 + 2\frac{C_{22}}{J_2}\right) \tag{A30b}$$

when using the definitions of the degree 2 coefficients of the gravitational potential,

$$C_{22} = \frac{B-A}{4MR^2} \,, \tag{A31a}$$

$$J_2 = \frac{C-\bar{A}}{MR^2} = \frac{\bar{A}e}{MR^2} \,. \tag{A31b}$$

Equation (A17) can thus be written as

$$(1+\omega)\left[(1+e)\tilde{p} + \tilde{m} + \frac{\bar{A}_f}{\bar{A}}\tilde{m}_f + \frac{\bar{A}_s}{\bar{A}}\tilde{m}_s + \frac{\bar{A}_s}{\bar{A}} e_s \alpha_3 \tilde{n}_s\right] = -\beta\Phi_1 - \beta\Phi_2\tilde{p} - \frac{\bar{A}_s}{\bar{A}} e_s \alpha_3 \Phi_2 \tilde{n}_s \,. \tag{A32}$$

This equation determines the tilt angle $\tilde{p}$ of the symmetry axis of the mantle with respect to the ecliptic plane. It is the equation that determines the Cassini state for the mantle, taking into account the misalignments of the rotation vectors of each region and the tilt of the inner core with respect to the mantle.

The external torque given by equation (A27) is the same as that of equation (A12) which applies on the right-hand side of equation (A16). Thus, the definition of $\tilde{\phi}$ given by equation (A28) can be substituted in equation (A16). In the system of equations (A16), we also need the torque from Earth acting on the inner core, which is given by the second term of equation (A25),

$$\tilde{\Gamma}_s^E = -i\frac{3}{2}\frac{n^2}{(1-e_L)^{3/2}}\left[\bar{A}_s e_s \alpha_3\right]\sin(I+\theta_p+\theta_s)\cos(I+\theta_p+\theta_s) \,. \tag{A33}$$

Assuming once again small tilt angles, we use $\theta_p \approx \tilde{p}, \theta_s \approx \tilde{n}_s$, and the approximation given by equation (A26b) so the torque can be expanded as

$$\tilde{\Gamma}_s^E = -i\Omega_o^2 \bar{A}_s e_s \alpha_3 \tilde{\phi}_s \,, \tag{A34}$$

which defines the parameter $\tilde{\phi}_s$ that we introduced in equation (A13) as

$$\tilde{\phi}_s = \Phi_1 + \Phi_2\tilde{p} + \Phi_2\tilde{n}_s \,. \tag{A35}$$

The substitution of $\tilde{\phi}$ and $\tilde{\phi}_s$ into the right-hand side of equations (A16) and the addition of equation (A32) to this system gives the linear system of five equations and five unknowns that is expanded in equations (5) and (6) of the main text.

As a final remark, one can notice the similarity between the two equations we have used to describe the angular momentum of the full Moon, one expressed in the ecliptic frame (equation (A32)), the other in the mantle frame (equation (A16)). These can be written, respectively, as

$$(1+\omega)\left[(1+e)\tilde{p}+\tilde{m}\right] = -(1+\omega)\left[\frac{\bar{A}_f}{\bar{A}}\tilde{m}_f + \frac{\bar{A}_s}{\bar{A}}\tilde{m}_s + \frac{\bar{A}_s}{\bar{A}}e_s\alpha_3\tilde{n}_s\right] - \tilde{\phi}\,, \tag{A36a}$$

$$(\omega-e)\tilde{m} = -(1+\omega)\left[\frac{\bar{A}_f}{\bar{A}}\tilde{m}_f + \frac{\bar{A}_s}{\bar{A}}\tilde{m}_s + \frac{\bar{A}_s}{\bar{A}}e_s\alpha_3\tilde{n}_s\right] - \tilde{\phi}\,. \tag{A36b}$$

The right-hand sides of these equations being equal, equating the left-hand sides gives a relationship between $\tilde{p}$ and $\tilde{m}$ for a forcing at a given frequency ω:

$$\tilde{p} = -\frac{\tilde{m}}{1+\omega}\,. \tag{A37}$$

This relationship was given by *Mathews et al.* [1991a, their equation (27)], where in the context of Earth, $\tilde{p}$ represents the amplitude of nutation (i.e., the displacement of the mantle symmetry axis with respect to the ecliptic normal). The factor $1+\omega$ that relates $\tilde{p}$ and $\tilde{m}$ has been referred to as the "wobble factor" by *Smith* [1977, his equation 2.15]. Equation (A37) expresses a fundamental kinematic relationship between $\tilde{p}$ and $\tilde{m}$, independent of the structure and composition of the planetary body considered.

The same relationship was also presented by *Eckhardt* [1981] in his seminal work on the Moon's libration. He showed that it derives from the invariance of the unit vector pointing toward the ecliptic normal in the inertial frame: the relationship of equation (A37) follows when considering the time changes of this unit vector in a frame rotating with the Moon (his equation 4, though note the sign difference with our definition of $\tilde{p}$).

The fact that our two different equations for the angular momentum of the Moon are consistent with the relationship between $\tilde{p}$ and $\tilde{m}$ is reassuring. Further, it suggests that rather than keeping each of these two equations, an alternative strategy is to eschew one and use equation (A37) to eliminate $\tilde{p}$ or $\tilde{m}$ so as to reduce equations (5) and (6) of the main text to a system of four equations and four unknowns.

Acknowledgments
The authors wish to thank Jim Williams and an anonymous reviewer for comments and suggestions that improved this paper. M.D. was supported by a NSERC/CRSNG discovery grant. M.W. was supported by a grant from the French space agency, CNES. All data for this paper are properly cited and referred to in the reference list.

References

Araki, H., et al. (2009), Lunar global shape and global and polar topography derived from Kaguya-LALT laser altimetry, *Science*, *323*, 897–900.
Baland, R.-M., M. Yseboodt, and T. Van Hoolst (2012), Obliquity of the Galilean satellites: The influence of a global internal liquid layer, *Icarus*, *220*, 435–448.
Bills, B. (2005), Free and forced obliquities of the Galilean satellites of Jupiter, *Icarus*, *175*, 233–247.
Buffett, B. A. (1992), Constraints on magnetic energy and mantle conductivity from the forced nutations of the Earth, *J. Geophys. Res.*, *97*, 19,581–19,597.
Buffett, B. A., P. M. Mathews, and T. A. Herring (2002), Modeling of nutation-precession: Effects of electromagnetic coupling, *J. Geophys. Res.*, *107*(B10), 2214, doi:10.1029/2001JB000056.
Colombo, G. (1966), Cassini's second and third laws, *Astron. J.*, *71*, 891–896.
Dickey, J. O., et al. (1994), Lunar laser ranging: A continuing legacy of the Apollo program, *Science*, *265*(5171), 482–490.
Dumberry, M., and L. Koot (2012), A global model of electromagnetic coupling for nutations, *Geophys. J. Int.*, *191*, 530–544.
Dwyer, C. A., D. J. Stevenson, and F. Nimmo (2011), A long-lived lunar dynamo driven by continuous mechanical stirring, *Nature*, *479*, 212–214.
Dziewonski, A. M., and D. L. Anderson (1981), Preliminary reference Earth model, *Phys. Earth Planet. Inter.*, *25*, 297–356.
Eckhardt, D. (1981), Theory of the librations of the Moon, *Moon Planets*, *25*, 3–49.
Garcia, R. F., J. Gagnepain-Beyneix, S. Chevrot, and P. Lognonné (2011), Very preliminary reference Moon model, *Phys. Earth Planet. Inter.*, *188*(1–2), 96–113, doi:10.1016/j.pepi.2011.06.015.
Getino, J., J. M. Farto, and J. M. Ferrandiz (1998), Obtaining the free frequencies of the non-rigid Earth, *Celest. Mech. Dyn. Astron.*, *71*, 95–108.
Gleason, A. E., and W. L. Mao (2013), Strength of iron at inner core pressures and evidence for a weak Earth's inner core, *Nat. Geosci.*, *6*, 571–574.
Goldreich, P. (1967), Precession of the Moon's core, *J. Geophys. Res.*, *72*, 3135–3137.
Gusev, A., and N. Petrova (2008), Project "The Moon—2012+": Spin-orbit evolution, geophysics and selenodesy of the Moon, *Adv. Space Res.*, *42*, 289–293.
Koot, L., and M. Dumberry (2011), Viscosity of the Earth's inner core: Constraints from nutation observations, *Earth Planet. Sci. Lett.*, *308*, 343–349.
Koot, L., M. Dumberry, A. Rivoldini, O. de Viron, and V. Dehant (2010), Constraints on the coupling at the core-mantle and inner core boundaries inferred from nutation observations, *Geophys. J. Int.*, *182*, 1279–1294.
Laneuville, M., M. A. Wieczorek, D. Breuer, J. Albert, G. Morard, and T. Rückriemen (2014), A long-lived lunar dynamo powered by core crystallization, *Earth Planet. Sci. Lett.*, *401*, 251–260, doi:10.1016/j.epsl.2014.05.057.
Le Bars, M., M. A. Wieczorek, O. Karatekin, D. Cébron, and M. Laneuville (2011), An impact-driven dynamo for the early Moon, *Nature*, *479*, 215–218.

Margot, J. L., S. J. Peale, S. C. Solomon, S. A. Hauck, F. D. Ghigo, R. F. Jurgens, M. Yseboodt, J. D. Giorgini, S. Padovan, and D. B. Campbell (2012), Mercury's moment of inertia from spin and gravity data, *J. Geophys. Res.*, *117*, E00L09, doi:10.1029/2012JE004161.

Mathews, P. M., B. A. Buffett, T. A. Herring, and I. I. Shapiro (1991a), Forced nutations of the Earth: Influence of inner core dynamics. 1. Theory, *J. Geophys. Res.*, *96*, 8219–8242.

Mathews, P. M., B. A. Buffett, T. A. Herring, and I. I. Shapiro (1991b), Forced nutations of the Earth: Influence of inner core dynamics. 2. Numerical results, *J. Geophys. Res.*, *96*, 8243–8257.

Mathews, P. M., T. A. Herring, and B. A. Buffett (2002), Modeling of nutations and precession: New nutation series for nonrigid Earth and insights into the Earth's interior, *J. Geophys. Res.*, *107*(B4), 2068, doi:10.1029/2004JB000390.

Meyer, J., and J. Wisdom (2011), Precession of the lunar core, *Icarus*, *211*, 921–924.

Peale, S. J. (1969), Generalized Cassini's laws, *Astron. J.*, *74*, 483–489.

Peale, S. J., J. L. Margot, S. A. Hauck II, and S. C. Solomon (2016), Consequences of a solid inner core on Mercury's spin configuration, *Icarus*, *264*, 443–455.

Poincaré, H. (1910), Sur la précession des corps déformables, *Bull. Astron. Ser.*, *1*(27), 321–356.

Rogister, Y., and B. Valette (2009), Influence of liquid core dynamics on rotational modes, *Geophys. J. Int.*, *176*, 368–388.

Scheinberb, A., K. M. Soderlund, and G. Schubert (2015), Magnetic field generation in the lunar core: The role of inner core growth, *Icarus*, *254*, 62–71, doi:10.1016/j.icarus.2015.03.013.

Smith, M. L. (1977), Wobble and nutation of the Earth, *Geophys. J. R. Astron. Soc.*, *50*, 103–140.

Tsujino, N., Y. Nishihara, Y. Nakajima, E. Takahashi, K. Funakoshi, and Y. Higo (2013), Equation of state of γ-Fe: Reference density for planetary cores, *Earth Planet. Sci. Lett.*, *375*, 244–253.

Veasey, M., and M. Dumberry (2011), The influence of Mercury's inner core on its physical libration, *Icarus*, *214*, 265–274.

Ward, W. R. (1975), Past orientation of the lunar spin axis, *Science*, *189*, 377–379.

Weber, R., P.-Y. Lin, E. J. Garnero, Q. Williams, and P. Lognonné (2011), Seismic detection of the lunar core, *Science*, *331*, 309–312.

Weiss, B. P., and S. M. Tikoo (2014), The lunar dynamo, *Science*, *346*(6214), 1246753, doi:10.1126/science.1246753.

Wieczorek, M. A., et al. (2006), The constitution and structure of the lunar interior, *Rev. Mineral. Geochem.*, *60*(6120), 221–364.

Wieczorek, M. A., et al. (2013), The crust of the Moon as seen by GRAIL, *Science*, *339*(6120), 671–675, doi:10.1126/science.1231530.

Williams, J. G. (2007), A scheme for lunar inner core detection, *Geophys. Res. Lett.*, *34*, L03202, doi:10.1029/2006GL028185.

Williams, J. G., and D. H. Boggs (2015), Tides on the Moon: Theory and determination of dissipation, *J. Geophys. Res. Planets*, *120*, 689–724, doi:10.1002/2014JE004755.

Williams, J. G., D. H. Boggs, C. F. Yoder, J. T. Ratcliff, and J. O. Dickey (2001), Lunar rotational dissipation in solid body and molten core, *J. Geophys. Res.*, *106*, 27,933–27,968.

Williams, J. G., D. H. Boggs, and J. T. Ratcliff (2014a), Free libration modes of a structured Moon, Abstract 1579 presented at 45th Lunar and Planetary Science Conference, The Woodlands, Tex., 16–20 March.

Williams, J. G., et al. (2014b), Lunar interior properties from the GRAIL mission, *J. Geophys. Res. Planets*, *119*, 1546–1578, doi:10.1002/2013JE004559.

Williams, J. G., A. S. Konopliv, R. S. Park, D.-N. Yuan, S. W. Asmar, D. E. Watkins, D. E. Smith, and M. T. Zuber (2015), The deep lunar interior from GRAIL, Abstract 1380 presented at 46th Lunar and Planetary Science Conference, The Woodlands, Tex., 16–20 March.

Yoder, C. F. (1981), The free librations of a dissipative Moon, *Philos. Trans. R. Soc. A*, *303*, 327–338.

Zhang, N., E. M. Parmentier, and Y. Liang (2013), A 3-D numerical study of the thermal evolution of the Moon after cumulate mantle overturn: The importance of rheology and core solidification, *J. Geophys. Res. Planets*, *118*, 1789–1804, doi:10.1002/jgre.20121.

Zuber, M., D. Smith, D. Lehman, T. Hoffman, S. Asmar, and M. Watkins (2013), Gravity Recovery and Interior Laboratory (GRAIL): Mapping the lunar interior from crust to core, *Space Sci. Rev.*, *178*, 3–24, doi:10.1007/s11214-012-9952-7.